

Handbook of Blind Source Separation,
Independent Component Analysis
and Applications

P. Comon and C. Jutten Eds



October 8, 2009

Chapter 18

ICA and biomedical applications

L. ALBERA, P. COMON, L.C. PARRA, A. KARFOUL, A. KACHENOURA, L. SENHADJI

In this chapter we focus on the use of Independent Component Analysis (ICA) in biomedical systems. Several studies dealing with ICA-based biomedical systems have been reported during the last decade. Nevertheless, most of these studies have only explored a limited number of ICA methods, namely SOBI [7], FastICA [39] and InfoMax [53]. In addition, the performance of ICA algorithms for arbitrary electro-physiological sources is still almost unknown. This prevents us from choosing the best method for a given application, and may limit the role of these methods in biomedical systems.

To overcome these limitations, the purpose of our study is first to show the interest of ICA in biomedical applications such as the analysis of human electro-physiological signals. Next, we aim at studying twelve of the most widespread ICA techniques in the signal processing community and identify those that are most appropriate for biomedical signals.

18.1 Introduction

The previous chapters presented various categories of algorithms to perform ICA. The main difference between the various methods lies in their approach for measuring statistical independence between random variables. One group of algorithms such as InfoMax [35], FastICA [38] or PICA [48] measure independence using Mutual Information (MI), which is directly related to the definition of independence via the Kullback-Leibler divergence [6]. Alternatively, algorithms use the normalized Differential Entropy (DE), which is a special distance to normality also referred to as negentropy (see chapter 3 page 102 or chapter 6

page 203 for a brief description). More precisely, the InfoMax method solves the ICA problem by maximizing the DE of the output of an invertible non-linear transform of the expected sources using the natural gradient algorithm [35] (see chapter 6 for more details). The PICA algorithm uses the parametric Pearson model in the score function in order to minimize the MI. Using either a deflation or a simultaneous optimization scheme, FastICA extracts each component by maximizing an approximation of the DE of the expected source by means of an approximate Newton iteration (which actually often reduces to a fixed-step gradient, as shown in section 6.10.4).

Another group of algorithms measure independence indirectly via cumulants which are easier to compute [59, 3, 2, 49] (see chapter 3). These statistical measures are very useful to build a good optimization criterion, referred to as contrast [19, definition 5]. This comes essentially from two important properties: i) if at least two components or groups of components are statistically independent, then all cross-cumulants involving these components are zero and ii) if a variable is Gaussian, then all its High Order (HO) cumulants are zero. Note that cross-cumulants share two other useful properties. For real-valued random variables they are symmetric matrices since the value of their entries does not change with the permutation of their indices, and they satisfy the multi-linearity property [59] (see also chapter 9 page 357).

Thus, numerous cumulant-based techniques were proposed such as JADE [10, 11], COM2 [18, 19], COM1 [21, 20], SOBI in both conventional [7] and robust whitening [105] versions, STOTD [52], SOBIUM [51], TFBSS [36, 30] and FOBIUM_{ACDC}. For more detailed description, one can refer to chapter 5 for methods COM2, JADE and STOTD, to chapter 7 for the SOBI algorithm, to chapter 9 for the SOBIUM method and to chapter 11 for the TFBSS approach. In the SOBI and TFBSS algorithms, ICA is solved by jointly diagonalizing several Second Order (SO) cumulant matrices, say covariance matrices, well-chosen in the time and the time-frequency planes, respectively. Also based on SO cumulants, the SOBIUM algorithm extends the SOBI concept to the case of under-determined mixtures (i.e. more sources than sensors). Regarding the FOBIUM_{ACDC} method, it is based on a non-orthogonal joint diagonalization of several Fourth Order (FO) cumulant matrices, well-known as quadricovariance matrices, using the diagonalization ACDC scheme [100].

It is noteworthy that the FOBIUM_{ACDC} method is a variant of FOBIUM [29], which has the advantage of processing both sub- and super-Gaussian sources. As far as the COM2 method is concerned, a maximization of a FO contrast function is used to extract independent components. In addition, the JADE algorithm [10] solves the ICA problem by jointly diagonalizing a set of eigenmatrices of the quadricovariance matrix of the whitened data. Following the same spirit as the JADE algorithm, STOTD [52] jointly diagonalizes third order slices extracted from the FO cumulant array of the whitened data.

We stress out that, a good performance of each technique is subject to some specific conditions or assumptions on the processed sources and the additive noise. For instance some methods require sources to be colored (i.e. temporarily correlated); others do not allow Gaussian noise with unknown spatial coherence, etc. Figure 18.1 sheds light on the essential hypothesis for each method considered in this chapter, and for which a good behavior is guaranteed.

This specific chapter aims at giving some insights into the numerical complexity of many of these ICA algorithms. In addition, it will give a comparative performance analysis based on simulated signals in electro-encephalography. Hopefully this chapter would provide useful reference for researchers from the biomedical community, especially for those who are not familiar with ICA techniques.

<i>Characteristics</i> <i>Algorithms</i>	Stat. order	Whitening	Allowed Gaussian sources	Necessity of source cumulants of the same sign	Necessity of sources with different spectrums	Utilization of the source coloration	Utilization of the source non-stationarity	Noise with unknown spatial coherence
SOBI	2	Yes	All	No	Yes at order 2	Yes	No	No
SOBI_{rob}	2	Yes (Robust)	All	No	Yes at order 2	Yes	No	No
TFBSS	2	Yes	All	No	Yes at order 2	Yes	Yes	No
SOBIUM	2	No	All	No	Yes at order 2	Yes	No	No
COM2	4	Yes	1	No	No	No	No	No
JADE	4	Yes	1	No	No	No	No	No
FOBIUM_{ACDC}	4	No	0	No	Yes at order 4	Yes	No	Yes if Gauss.
STOITD	4	Yes	1	No	No	No	No	No
FastICA_{sym}	4	Yes	1	No	No	No	No	No
FastICA_{def}	4	Yes	1	No	No	No	No	No
PICA	Up to 4	Yes	1	No	No	No	No	No
INFOMAX	4	Yes	1	No	No	No	No	No

Figure 18.1: Twelve ICA methods with their main characteristics

18.2 One decade of ICA-based biomedical data processing

Advances in data recordings technologies and digital signal processing have enabled recordings and analysis of vast amounts of multidimensional biomedical data. The extraction of the essential features from the data becomes therefore paramount. The use of ICA in biomedical systems is now very widespread since the ICA concept is very easy to understand: it decomposes the data as a linear combination of statistically independent components. However, biomedical signals pose a challenge as it is often difficult to ascertain a ground truth that could be used to evaluate the accuracy of the ICA decomposition, or even its meaning. The following questions therefore deserve careful consideration: Can the data be modeled as a linear combination of physically independent random processes? Are there a fixed and known number of such independent processes? Do they represent independent source signals or more generally independent source subspaces? The answers to these questions are not simple and thus the results of ICA for biomedical signals requires often a significant level of interpretation and expert knowledge. This section will survey biomedical applications where ICA plays a central role to provide an overview of the assumptions and motivations for its use.

18.2.1 Electromagnetic recordings for functional brain imaging

As explained in [4], functional brain imaging is a relatively new and multidisciplinary research field that encompasses techniques devoted to a better understanding of the human brain through noninvasive imaging of the electrophysiological, hemodynamic, metabolic, and neurochemical processes that underlie normal and pathological brain function. These imaging techniques are powerful tools for studying neural processes in the normal working brain. Clinical applications include improved understanding and treatment of serious neurological and neuropsychological disorders such as intractable epilepsy, schizophrenia, depression, Parkinson's disease and Alzheimer's disease. Due to the unsurpassed temporal resolution of electro-encephalography (EEG) and magneto-

encephalography (MEG), and to their widespread use by clinicians and scientists, we decided to focus on these both functional brain imaging tools.

EEG and MEG are two complementary techniques that measure, respectively, the scalp electric potentials and the magnetic fields outside the head produced by currents in neural cell assemblies (figure 18.2). They directly mea-

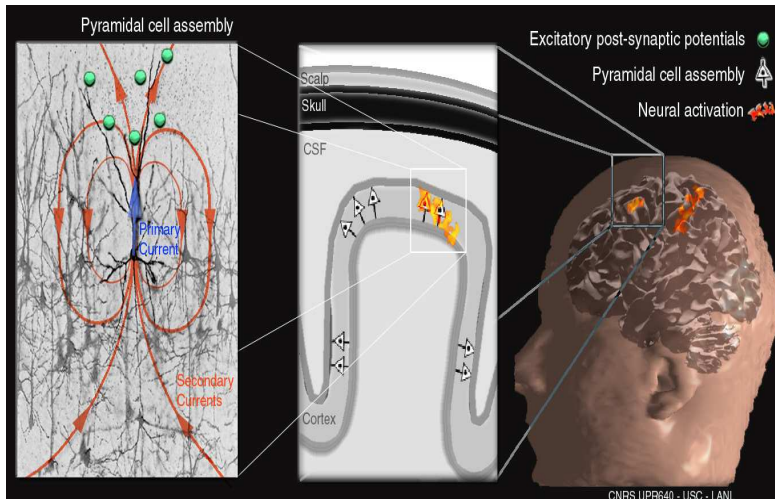


Figure 18.2: Left: Excitatory postsynaptic potentials (EPSPs) are generated at the apical dendritic tree of a cortical pyramidal cell and trigger the generation of a current that flows through the volume conductor from the non-excited membrane of the soma and basal dendrites to the apical dendritic tree sustaining the EPSPs. Some of the current takes the shortest route between the source and the sink by traveling within the dendritic trunk (primary current in blue), while conservation of electric charges imposes that the current loop be closed with extracellular currents flowing even through the most distant part of the volume conductor (secondary currents in red). Center: Large cortical pyramidal nerve cells are organized in macro-assemblies with their dendrites normally oriented to the local cortical surface. This spatial arrangement and the simultaneous activation of a large population of these cells contribute to the spatio-temporal superposition of the elemental activity of every cell, resulting in a current flow that generates detectable EEG and MEG signals. Right: Functional networks made of these cortical cell assemblies and distributed at possibly multiple brain locations are thus the putative main generators of MEG and EEG signals. From [4] with permission.

sure electrical brain activity and allow for studies of the dynamics of neural networks or cell assemblies that occur at typical time scales on the order of tens of milliseconds as shown in figure 18.3. EEG was born in 1924 when the German physician Hans Berger first measured traces of brain electrical activity in humans. Although today's electronics and software for EEG analysis benefit from the most recent technological developments, the basic principle remains unchanged from Berger's time. EEG consists of measurements of a set of electric potential differences between pairs of scalp electrodes. The sensors may be either directly glued to the skin (for prolonged clinical observation) at selected locations directly above cortical regions of interest or fitted in an elastic cap for rapid attachment with near uniform coverage of the entire scalp. Research protocols can use up to 256 electrodes. In many clinical and research applications, EEG data are analyzed using pattern analysis methods to associate

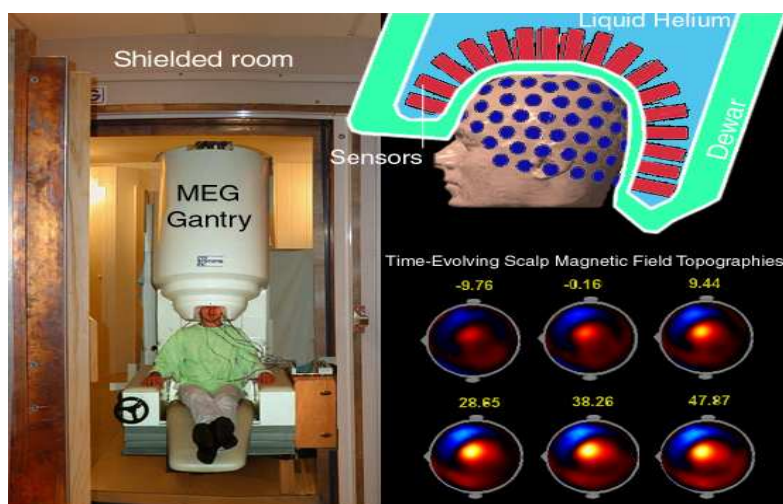


Figure 18.3: Typical scalp magnetic fields are on the order of a 10 billionth of the earth’s magnetic field. MEG fields are measured inside a magnetically shielded room for protection against higher-frequency electromagnetic perturbations (left). MEG sensors use low-temperature electronics cooled by liquid helium (upper right) stored in a Dewar (left and upper right). Scalp magnetic fields are then recorded typically every millisecond. The resulting data can be visualized as time-evolving scalp magnetic field topographies (lower right). These plots display the time series of the recorded magnetic fields interpolated between sensor locations on the subject’s scalp surface. This MEG recording was acquired as the subject moved his finger at time 0 (time relative to movement ($t=0$) is indicated in ms above every topography). Data indicate early motor preparation prior to the movement onset before peaking at about 20 ms after movement onset. From [4] with permission.

characteristic differences in the data with differences in patient populations or experimental paradigm. Typical EEG scalp voltages are on the order of tens of microvolts and thus readily measured using relatively low-cost scalp electrodes and high-impedance high-gain amplifiers.

In contrast, characteristic magnetic fields produced by neural currents are extraordinarily weak, on the order of several tens of femtoTeslas, thus necessitating sophisticated sensing technology. MEG was developed in physics laboratories and especially in low-temperature and superconductivity research groups. In the late 1960s, Zimmerman co-invented the SQUID (Superconducting QUantum Interference Device)—a supremely sensitive amplifier that has since found applications ranging from airborne submarine sensing to the detection of gravitational waves—and conducted the first human magnetocardiogram experiment using a SQUID sensor at MIT. SQUIDs can be used to detect and quantify minute changes in the magnetic flux through magnetometer coils in a superconducting environment. Cohen, also at MIT, made the first MEG recording a few years later [17]. Recent developments include whole-head sensor arrays for the monitoring of brain magnetic fields at typically 100 to 300 locations.

To our knowledge, Makeig et al. [56] and Vigario [89] were the first to apply ICA to EEG data. Now ICA is widely used in the EEG/MEG research community [56, 89, 90, 93, 92, 84, 85, 94, 65, 31, 69, 37, 47, 91, 22, 47, 40, 43, 45, 44, 41, 25, 57, 63]. Applications of ICA mainly include artifact detection and removal [85, 65, 69, 37, 40, 43, 45, 44, 92, 41, 89], analysis of event-related

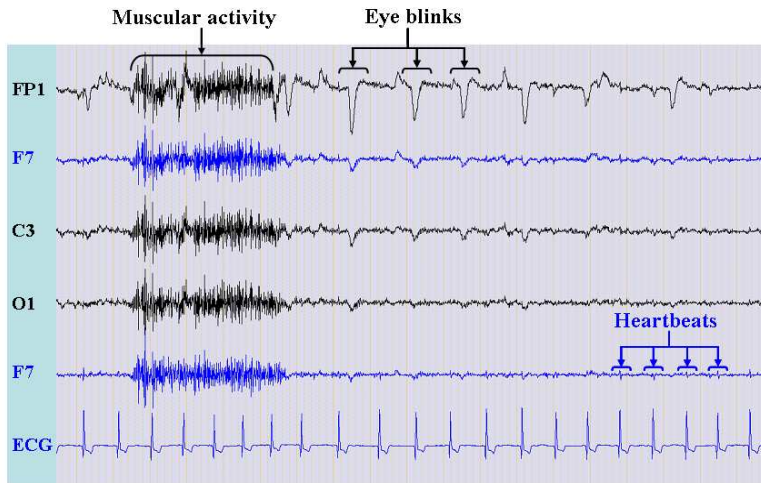


Figure 18.4: Some surface electrical activities recorded by a few EEG electrodes, derived from the standardized 10-20 system, and an ECG sensor.

response averages [92, 56, 45, 44, 57], and single-trial EEG/MEG [84, 45, 25, 63]. In order to illustrate more precisely the use of ICA, two applications are discussed in the sequel. The latter are devoted to the denoising problem in EEG and MEG, respectively. Such a problem plays an important role in the analysis of electromagnetic recordings.

Indeed, the signals of interest are very often recorded in the presence of noise signals, which can be decomposed into the sum of internal and external noises. The external noise is the instrumentation noise. The internal “noise” comprises all normal physiological activity that may generate electrical currents but that is not of interest to a specific study. A common example of physiological noise is the activity elicited by movements of the eyes and eye blinks [89]. Similarly, jaw-muscle activity caused by chewing or talking leads to large broad-band signals that overshadow the more subtle brain signals. Figure 18.4 displays a few channels of EEG signals contaminated by such artifacts – the naming convention for the different channels is based on the standardized 10-20 system (figure 18.19). The cardiac cycle, as well as contamination coming from a digital watch (see [91, figure 3]), can also disturb the EEG/MEG signals of interest.

Choosing an inactive voltage reference for recording is one of the oldest technical problems in EEG. Since commonly used cephalic references contaminate EEG and can lead to misinterpretation, the elimination of the reference contribution is of fundamental interest. That is the purpose of the work presented in [37] by applying ICA to interictal recordings. In fact, the classical EEG recording techniques may complicate the extraction of accurate information. For instance, in coherence analysis the presence of a common reference signal in EEG recordings results in a distortion of the synchrony values observed and may destroy the intended physical interpretation of phase synchrony [78, 34].

Other montages such as bipolar EEG, average common reference EEG and Laplacian EEG can be used in order to obtain reference-free EEG. But all of them also present strong drawbacks. The bipolar EEG, obtained by subtracting the potentials of two nearby electrodes, will remove all signals common to the two channels, including the common reference but also information from dipoles with certain locations and tangential orientations. The average reference EEG, obtained by subtracting the average of all recording electrodes (i.e. the average

reference) from each channel does not suit the classical 10 – 20 system coverage [46, 34] and would need a denser coverage of the head surface [46] to be really efficient. Eventually, Laplacian maps, based on the second spatial derivative in an attempt to remove non-local contributions to the potential, eliminate all the distributed sources regardless whether or not they originate from the reference and are biased toward superficial, radial sources. In addition, the three latter techniques can also lead to misinterpretation of the synchronization results.

In order to overcome the drawbacks of the classical methods, Hu et al. proposed to use ICA for identification and removal of the reference signal contribution from intracranial EEG (iEEG) recorded with a scalp reference signal. All EEG potential measurements reflect the difference between two potentials, and can then be factorized as a static mixture of two source subspaces corresponding to the reference signal and signals of interest, respectively. The former subspace is 1-dimensional by definition, while the latter subspace may have a higher dimension. As far as the statistical independence between both subspaces is concerned, as mentioned by the authors, it should at least be approximately true because of the high resistivity of the skull between scalp electrode and intracranial electrodes. Then the FastICA method is used in order to automatically extract the scalp reference signal based on its independence with the bipolar iEEG data. When iEEG and scalp EEG (figure 18.5(a)) are recorded simultaneously using the same scalp reference, the scalp reference signal R_2 extracted by ICA from iEEG can also be used in order to clean the scalp EEG. The results of the latter procedure are displayed in figure 18.5(c) in comparison with other techniques such as bipolar scalp EEG (figure 18.5(b)) and average reference scalp EEG (figure 18.5(d)). The R_2 corrected EEG is clearly advantageous over the average reference corrected. The average reference corrected EEG in this case has removed the diffuse cerebral activity that remains evident in the R_2 corrected EEG. The R_2 corrected EEG is also advantageous over the bipolar EEG because the bipolar EEG usually leads to smaller amplitudes (see for instance F7-T7 in figure 18.5(c) and F7 and T7 in figure 18.5(b)) and causes misinterpretation of EEG.

MEG is useful in preparation of epilepsy surgery in order to localize current dipoles from surface epileptic spikes allowing for cortex mapping and intracranial electrodes placement. As a result, several approaches for epileptic spike detection were proposed such as morphological analysis, template matching, predictive filtering and ICA analysis (see [65] and the references therein). In practice these techniques have various limitations. For instance, methods based on morphological analysis and template matching do not take into account the spatial structure of the measurements since they were developed for single channel data [65]. Predictive filtering techniques are less appropriate for MEG data since they were basically proposed for EEG recordings well-known to have a better SNR [65].

Now concerning spike detection techniques, the majority of them requires visual inspection or interpretation of independent components and manual cluster analysis to discard spurious sources [65]. In order to overcome these drawbacks, Ossadtchi et al. proposed the use of ICA in a fully automated way [65]. It is noteworthy that the latter authors jointly identify the epileptic spikes and the corresponding current dipole positions in an efficient way.

First, an ICA analysis via the InfoMax algorithm [35] is used to recover the spike-like components from MEG measurements assumed to correspond to a noisy static mixture of two statistically independent source subspaces, say, focal epileptic and background activity sources interfered with a spatially independent instrumentation noise. The static mixture assumption is justified by the quasistatic electromagnetic properties of MEG data. In our opinion, the independence assumption between the three classes of signals holds true in practice

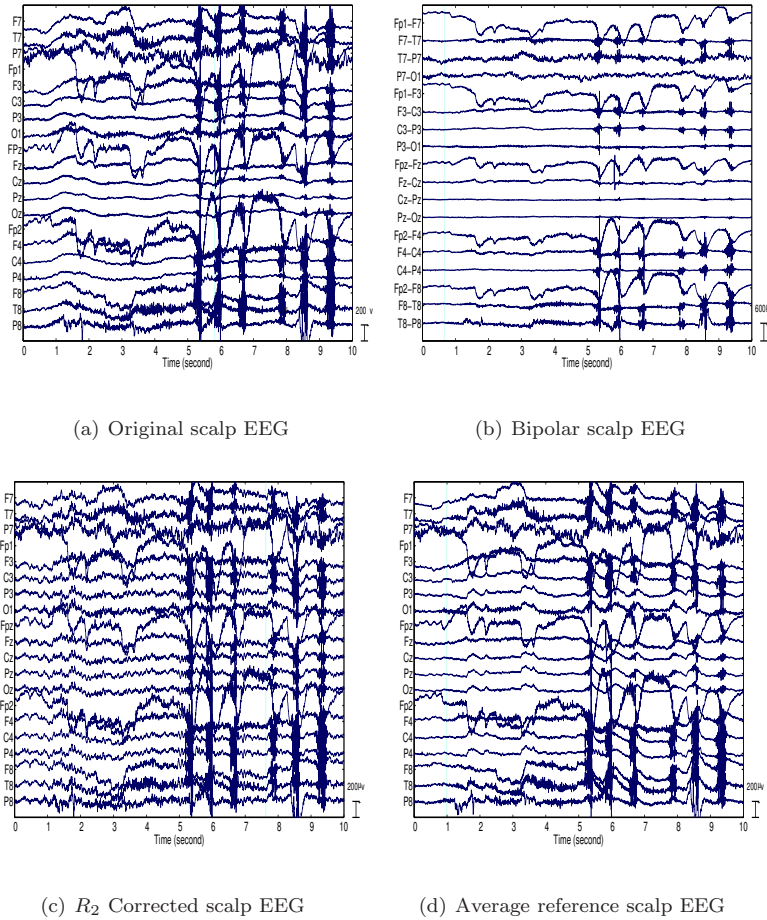


Figure 18.5: Removal of the reference contribution from scalp EEG recorded simultaneously with iEEG using the same scalp reference. (a) A 10-s sample of scalp EEG recorded simultaneously with iEEG using the same scalp reference. The segment is remarkable for the large muscle artifact due to the patient chewing between 5 s and 10 s. (b) Bipolar scalp EEG is created by subtracting the EEG signal from adjacent electrodes. This demonstrates that in this case the muscle artifact is not only from the common scalp reference. (c) The corrected scalp EEG using R_2 to remove the reference contribution. (d) The scalp EEG obtained using the average scalp reference. From [37] with permission.

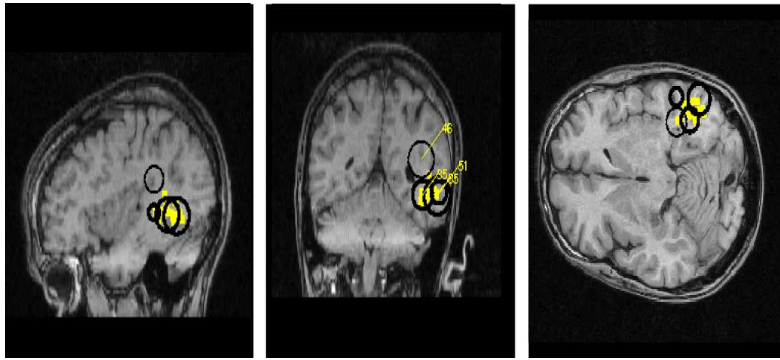


Figure 18.6: Manual (yellow square dots) and automated (circles) detection and clustering results for one subject. From [65] with permission.

due to i) the macroscopic desynchronization between the neurons contributing to the epileptic spikes and those contributing to the background activity, and ii) the physical independence between intracerebral activities and instrumentation noise.

Second, a spikiness index is used to select the components with spike-like characteristics among all those extracted by InfoMax and only the most spiky sources are retained in order to reconstruct a denoised epileptic surface of MEG data. Then, a focal neuronal source localization step is realized on these new surface data by means of the RAP-MUSIC algorithm [62] where the current dipole model is fitted in the vicinity of each previously detected spike (i.e. with a temporal window of size 16 ms). As a result, the retained spiky sources are those that fit a current dipole with more than 95%. Next, a clustering procedure is applied on all localized dipoles in order to reduce the number of detected spiky sources. The retained sources are those falling within one of clusters automatically determined using a distance metric taking into account both the location and the time courses of the considered sources. Finally, a cluster significance step based on a statistical test is used to refine the results by excluding all non statistically significant clusters among all those defined in the previous step. This elaborate process is a good example of the type of expert knowledge that is sometimes required when interpreting the results of ICA on biomedical signals.

The proposed method showed similar performance in terms of abnormal activity detection compared to the one using the conventional four phases clinical procedure performed on four subjects requiring invasive electrode recordings for localization of the seizure origin for surgical planning. For one of the four considered subjects, figure 18.6 shows the performance of the proposed method (circles) for both abnormal spike activity detection and its spatial location determination. Reported results were compared to a manual detection performed by a qualified examiner (yellow square dots) [65]. Probable epileptogenic clusters were referred by circles with thicker lines while thinner lines indicate non-epileptogenic clusters as determined by their location and averaged time courses. On the other hand, in order to evaluate the necessity of spatial and temporal investigation of putative clusters of localized sources during the clustering step, two different clusters were studied in figures 18.7 and 18.8, respectively. Figure 18.7 shows the average time course of dipoles localized in the temporal lobe. Due to its spike-like shape, the investigated cluster was retained as a result. But, the inspection of the average time course of the second cluster in figure 18.8 shows a less-descriptive spike-like characteristic, hence its elimination.

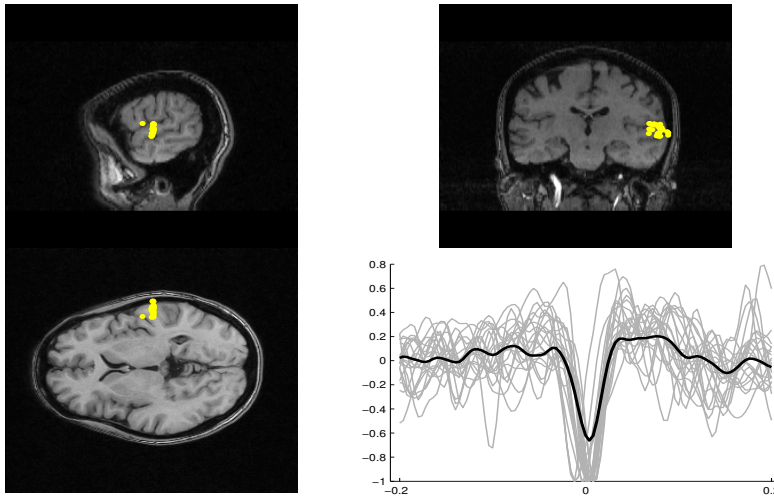


Figure 18.7: Location in three orthogonal views of an apparent dipole cluster (cluster 1) found for one subject. This cluster was retained by the method since its average time course represents a potentially epileptogenic region. From [65] with permission.

18.2.2 Electrocardiogram signal analysis

The electrocardiogram (ECG) reflects the electrical activity of the heart which is usually recorded with surface electrodes placed on the chest, arms and limbs. A typical ECG signal of a normal heartbeat (figure 18.9) is composed by a series of waves, namely, the P-wave which describes the sequential depolarization of the right and the left atria, the QRS complex is related to the depolarization of the right and the left ventricles and the T-wave is generated by the ventricular repolarization [79]. In clinical practice, there are many systems to ECG signal acquisition [97, 79]. The standard 12-lead ECG seems to be the most widely used by the physicians especially when waveform morphology is required. It is obtained by placing two electrodes on the two hands (VR and VL), one electrode on the left foot (VF) and six precordial electrodes (V1 to V6). The positions of the nine electrodes are typically chosen to capture the electric activity of the heart from different angles reconstructing the spatial dynamics of the heart's electrical activity. Although the ECG recording techniques are very effective, the distortions caused by noises and artifacts are still very significant. Indeed, in many practical situations, the ECG signal is contaminated by different types of noises and artifacts, such as sinusoidal 50/60 Hz power-line, electrode movements and broken wire contacts, but also interfering physiological signals as those related to muscle movements and breathing. In addition, some arrhythmias may caused various disturbances in the regular rhythm of the heart and thus generate ECG waves which are very different from those of the normal heartbeats. Hence, the main objective in ECG signal analysis is two-fold: i) to denoise the ECG signal in order to enhance the SNR of the signals of interest and ii) to separate the different bioelectric sources of the heart, such as ventricular activity (VA) and atrial activity (AA), in order to characterize some specific arrhythmias.

Several approaches to ECG analysis have been reported such as linear noise filtering [71], adaptive filtering [96, 83, 86], neural network [99, 87] and wavelet transform [77]. The majority of these methods have various drawbacks. Cardiac signal often overlap with various sources of noises and artifacts in time and fre-

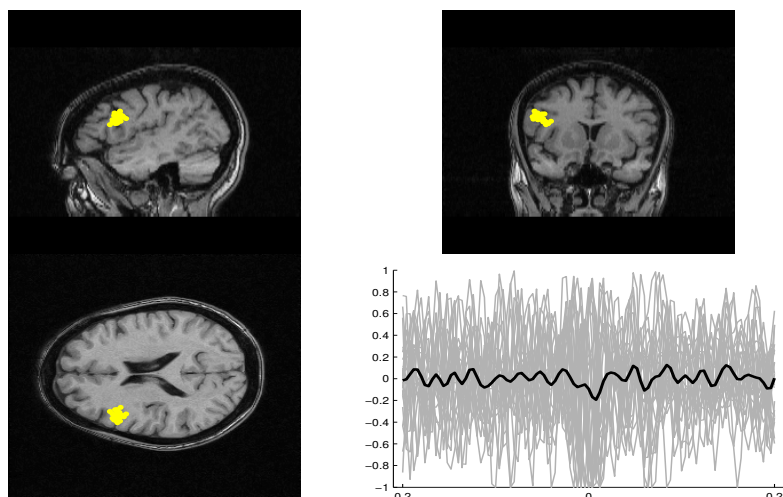


Figure 18.8: Location in three orthogonal views of an apparent dipole cluster (cluster 2) found for the same subject presented in figure 18.7. This cluster was discarded by the method since its average time course does not match with the an epileptogenic region activity. From [65] with permission.

quency domain. Thus extracting the signal of interest may be a difficult task. In addition, as noted in chapter 16, some of these methods usually need the use of reference signals, which make their performance highly dependent on the reference electrode positions. Due to these limitations, reliable signal processing tools for signal enhancement, detection and noise reduction are crucial for cardiac diagnosis and therapy. In contrast to the methods mentioned above, ICA has the potential of extracting signal sources even if they are superimposed in time-frequency. Moreover, ICA can estimate the sources by taking into account their spatio-temporal correlation, physiological prior information and their mutual statistical independence. Therefore, it appears natural to consider ICA techniques as a potential tool for ECG analysis. ICA has been applied to ECG with various purposes. These include artifact and noise removal [98, 5, 82, 14], analysis of the autonomic control of the heart [88], ventricular arrhythmia detection and classification [66], extraction of the Fetal ECG (FECG) from maternal recordings [23, 9, 24, 104] and the atrial activity extraction for Atrial Fibrillation (AF) [74, 72, 73, 12, 102]. To show how the ICA technique can be applied to ECG signal analysis, we discuss two of the most frequent applications in more detail, namely the extraction of fetal ECG and extraction of arterial activity.

The FECG can provide the clinician with valuable information on the well-being of the fetus and facilitates early diagnosis of fetal cardiac abnormalities and other pathologies. For instance, hypoxia may cause an alteration in the PR and the RR intervals [95], whereas a depression of the ST segment may be associated with acidosis [81]. Invasive recordings provide FECG with high SNR [67], but the procedure requires the use of intrauterine electrodes and is therefore only performed during labor when there is access to the fetal scalp. Non-invasive recordings with several electrodes placed on the mother's body can provide FECG. However, obtaining clean and reliable FECG is challenging due to the interfering ECG from the mother (MECG) and other interfering signals such as respiration, the electro-myogram (EMG), electrode movements and baseline drift. The mother's QRS wave occasionally overlaps with the fetal QRS wave making even visual detection of the individual beat of the fetus

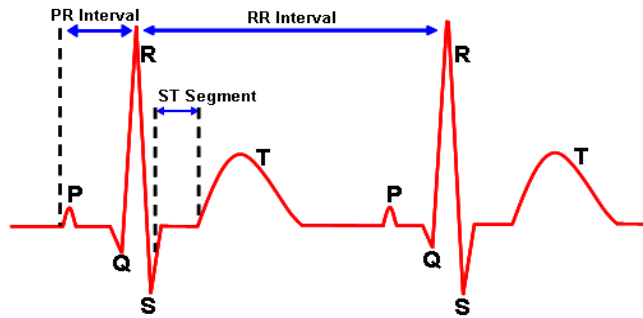


Figure 18.9: The ECG wave and its important features.

impossible, let alone any automated beat detection. Efforts to extract fetal ECG include adaptive filtering, linear decomposition of single and multi-channel recordings and nonlinear projection methods (see [76, chapter 2]) including ICA which we will discuss next.

De Lathauwer et al. [23] show that the separation of FECG from mother's skin electrodes can be approached as a linear instantaneous blind source separation problem. More precisely, the authors discuss two important aspects: i) the nature of the occurring signal and ii) the characteristics of the propagation from bioelectric sources to skin electrodes. Regarding the first aspect, the authors state in accordance with the work of [68] that the MECG-subspace is characterized by a three-dimensional vector signal, whereas the dimension of the FECG-subspace is subject to changes during the pregnancy period [68]. The transfer function between the bioelectric sources to body surface electrodes is assumed to be linear and resistive [64]. Finally, the high propagation velocity of the electrical signal in the human tissues validate the instantaneous assumption of the model. Authors show that the application of the ICA method proposed in [19] to eight ECG observations (see figure 16.17 in chapter 16) recorded from five skin electrodes located on mother's abdominal region (electrodes placed near the fetus) and three electrodes positioned near the mother's heart (on the mother's thoracic region) provides very interesting preliminary results (see section 16.7.1 for more details). A complete and extended study of [23] is presented by the same team in [24]. They investigate the case of atypical fetal heart rate (FHR) and the case of fetal twins. To do so, the FHR is artificially obtained using the real observations depicted in figure 16.17. More precisely, a small piece of data around $t = 0.75s$ in figure 16.17 was copied to $t = 3.5s$ to simulate an extrasystolic fetal heartbeat and the QRS wave around $t = 2s$ was removed. Figure 18.11 (a) illustrates that the application of ICA on the latter artificial observations succeeds in the extraction of FECG from multi-lead potential recordings on the mother's skin. Figure 18.10 shows an artificial observations of the fetal twins. The data of this figure were obtained by shifting both the sixth and the eighth components of figure 16.18 to artificially generate a new independent ECG attributed to the second fetus. These two signals were then merged with the original observations (figure 16.17) after multiplication with random mixing vectors. Figure 18.11 (b) shows that ICA is also able to discriminate the two fetal twins ECG subspaces, say components 6 and 8 for the first fetus and component 7 for the second fetus.

In [104], Zarzoso et al. compare a standard adaptive filtering method, namely multi-reference adaptive noise canceling (MRANC) [96] with the ICA discussed in method [103]. Figure 18.12 shows one of the cutaneous electrode recording used in the study. The first five channels correspond to the electrodes

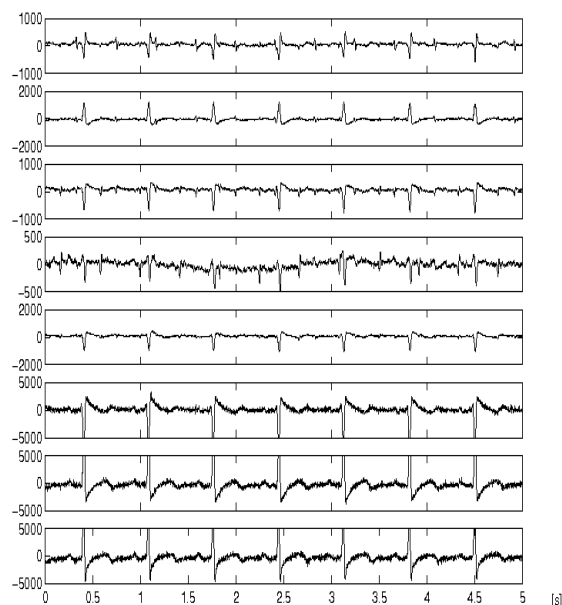
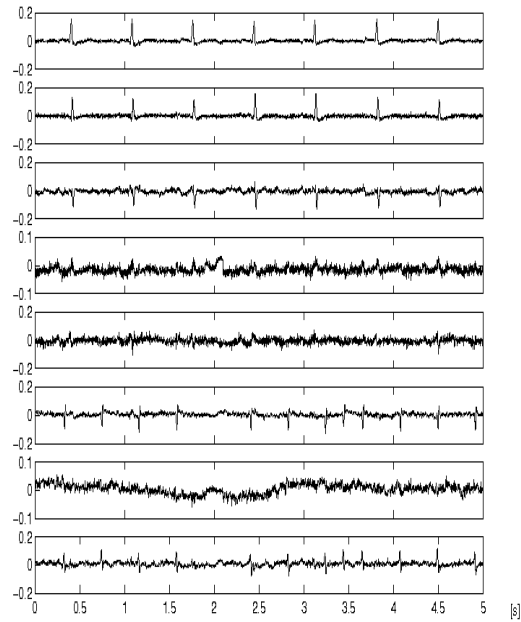


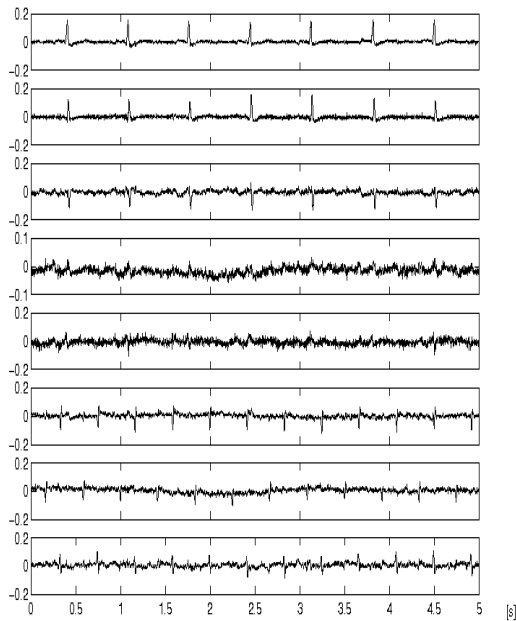
Figure 18.10: 8-channel set of observations containing heartbeats of fetal twins. From [24] with permission.

placed on the mother's abdominal region and the last three signals are related to the mother's chest electrodes. The results obtained with MRANC, using the three thoracic leads as reference are depicted in figure 18.13. Figure 18.14 displays the FECG contribution to the abdominal electrodes (first five signals) and to chest electrodes (last three signals) of the original recordings obtained with ICA. More precisely, the ICA method is first applied to the raw data to isolate the fetal subspace and then to reconstruct the surface FECG from the FECG-subspace only. Contrary to the MRANC method where the estimated components are still corrupted by the baseline drift (signal 4 of figure 18.13), the ICA method seems to be more effective to reconstruct the FECG contribution. Indeed, the baseline drift is eliminated in figure 18.14 and all fetal components are less noisy in comparison to those obtained by the MRANC method. It is also important to point out that, because ICA does not need to use reference signals, they are able to reconstruct the FECG contribution to the eight electrodes, either thoracic or abdominal.

Atrial fibrillation (AF) is one of the most common arrhythmias managed in human cardiology. In the general population it has a prevalence of 0.4 – 1%, increasing to around 9% among those over 80 years of age [16, 32]. AF is a supraventricular tachyarrhythmia characterized by uncoordinated atrial activation. The result is the replacement of the P waves by rapid oscillations or fibrillatory waves that vary in size, shape and timing [32]. AF is associated with increased mortality and hospitalization in the general population, and understanding of pathological mechanisms underlying AF using non-invasive diagnosis tools such as surface ECG is crucial to improve the patient treatment strategies. However, due to the low SNR of AA on surface ECG the analysis of AF remains difficult. Some methods reported in the literature to enhance AA involve direct suppression of QRS-T by subtracting: i) a fixed or adaptive template [86, 80] or ii) an estimated QRS-T complex [87]. Other approaches, based on Principal



(a)



(b)

Figure 18.11: (a) Source estimates obtained from data containing an extrasystole around $t = 3.5s$ and missing a fetal heartbeat around $t = 2s$ and (b) source estimates obtained from the data of figure 18.10. From [24] with permission.

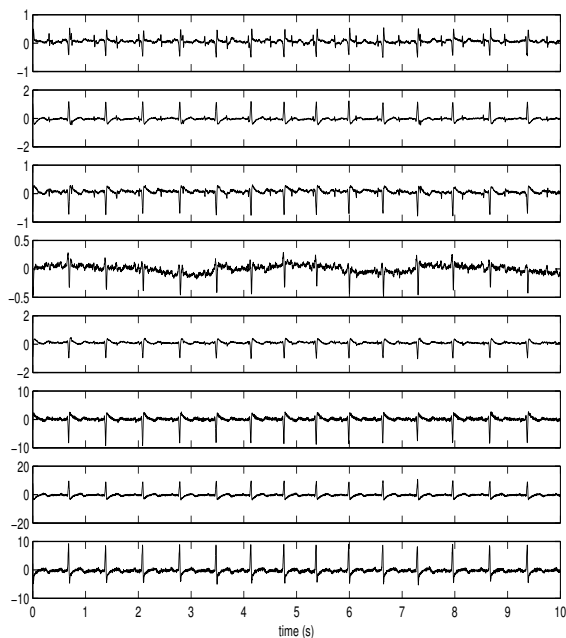


Figure 18.12: A cutaneous electrode recording from a pregnant woman. From [104] with permission.

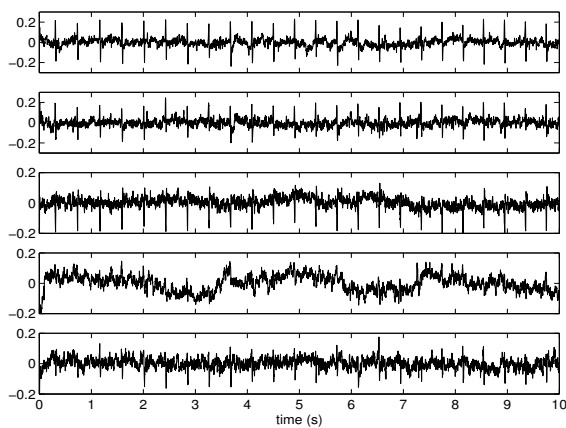


Figure 18.13: FECG contribution to the abdominal electrodes (first five signals) of figure 18.12 obtained by the MRANC method. From [104] with permission.

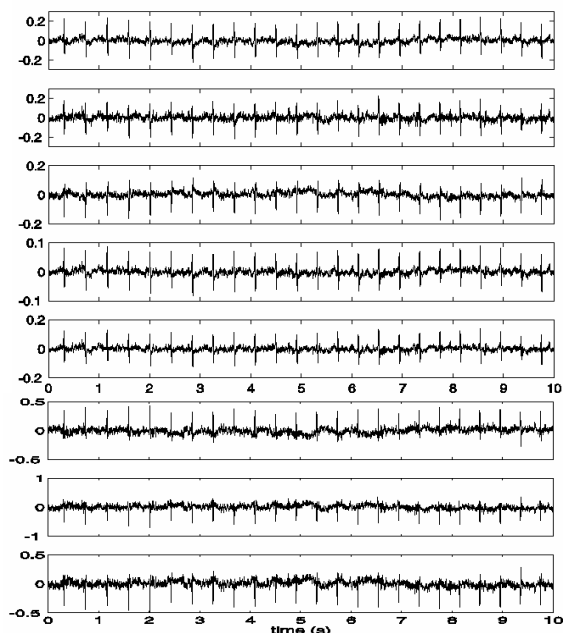


Figure 18.14: FECCG contribution to the abdominal electrodes (first five signals) and to the thoracic electrodes (last three signals) of figure 18.12 obtained with ICA. From [104] with permission.

Component Analysis (PCA) [50, 27, 54] try to derive a relatively small number of uncorrelated linear combinations (principal components) of a set of random zero-mean variables while retaining as much of the information from the data as possible [19, 26]. The major drawbacks of the QRS-T subtraction approaches are the use of a small number of QRS-T templates and the high sensitivity to QRS morphological changes. Regarding the PCA based methods, the orthogonality of the bioelectrical sources of the heart is not physiologically justified. This orthogonality condition can only be obtained through a correct orthogonal lead, known as the Frank lead system after its inventor [97, 79].

The AF problem was tackled by means of ICA-based methods in [73]. The authors justify three basic considerations regarding AA and VA, and the way which both activities are acquired from the surface electrodes: i) the independence of VA and AA, ii) their non-Gaussianity and iii) the observations follow an instantaneous linear mixing model. First, due to the bioelectrical independence of the atrial and ventricular regions [55], the atrial and ventricular electrical sources can reasonably be considered as statistically independent. Second, the distributions of AA and VA are sub-Gaussian and super-Gaussian, respectively (see section II.C [73] for more details). Finally, the bioelectric theory has modeled the torso as an inhomogeneous volume conductor [68, 58] which justifies that ECG surface recordings can be assumed to arise as a linear instantaneous transformation of cardiac bioelectric sources. Hence, the application of ICA-based methods to extract AA from 12-lead ECG seems to be well suited. The authors apply the FastICA algorithm [38] on the 12-lead ECG of seven patients suffering from AF, where they consider that the source subspace is composed of AA, VA and other interferences. The use of FastICA is justified by the fact that this algorithm demonstrates a very fast convergence and it can operate in a deflation mode (can be stopped as soon as the AA sources have been extracted).

Figure 18.15(a) displays a 12-lead ECG with an AF episode. Fibrillation waves are observed in several leads, especially leads II, III, aVF and V1. The results obtained after applying ICA are depicted on figure 18.15(b). The authors estimate the kurtosis of the extracted sources and show that the three first separated sources have a more sub-Gaussian distribution and hence are candidates to be related to AA. The sources 4 to 7 are associated with Gaussian noise and artifact, whereas the components 8 to 12 which present a super-Gaussian distribution contain a VA.

One important problem that arises when ICA is used in a biomedical context is to automatically select and classify independent sources of interest, as addressed in chapter 16 (section 16.7.3). Typically, in the above example the question is: how to choose the most informative AA sources among the three first extracted components of figure 18.15(b)? The authors solve this problem by exploiting some prior information about spectral content of AA during an AF episode. Indeed, the AA signal exhibits a narrow-band spectrum with a main frequency peak, f_p , between $3.5 - 9 \text{ Hz}$ [50]. Thus, they apply a spectral analysis over all the sources with sub-Gaussian distribution (kurtosis < 0) and choose the first component of figure 18.15(b) as the AA source because it presents a major peak at frequency $f_p = 6.31 \text{ Hz}$. The previous study only exploits the spatial diversity introduced by the different placement of the electrodes on the body. However, the exploitation of the temporal correlation of the AA source may improve the analysis of AF episode. Based on the narrow-band character of the AA, Castells et al. [12] propose a spatio-temporal blind source separation technique which takes advantage of both the spatial and the temporal information contained in the 12-lead ECG. This technique (figure 18.16) consists of an initial ICA step carried out by means of the FastICA algorithm [38] which aims to remove the non-Gaussian interferences such as VA sources. The second step, based on the SOBI algorithm [7], exploits the narrow-band nature of the AA source in order to improve its extraction from near-Gaussian source subspaces [102]. To evaluate the spatio-temporal ICA method, the authors simulate the synthesized ECG with a known AA source and then validate the results on 14 real-life ECGs AF data. The results obtained on the simulated database demonstrate the effectiveness of the spatio-temporal ICA method in comparison with spatial ICA [73]. Indeed, the correlation coefficients, between the real AA and the extracted AA, lie between 0.75 and 0.91, whereas the correlation coefficients of the spatial ICA method lie between 0.64 and 0.80. Regarding the real-life data, figure 18.17(a) shows that the estimated AA source provided by the spatio-temporal ICA method (bottom) seems to be less noisy in comparison to the AA source obtained by the spatial ICA technique (top). Figure 18.17(b) displays the spectral concentration around the main frequency peak, $f_p = 6.31 \text{ Hz}$, for the whole real-life database. The spectral concentration is computed as the percentage of the signal power in the frequency interval $[0.82f_p, 1.17f_p]$. According to this criterion, the spatio-temporal ICA method clearly outperforms the spatial-only ICA method.

18.2.3 Other application fields

It would be regrettable to close this bibliographical survey without citing other application fields such as functional Magnetic Resonance Imaging (fMRI) where ICA was used. Especially since fMRI was one of the first biomedical fields explored by ICA methods [60, 61]. In fact, fMRI is a technique that provides the opportunity to study brain function non-invasively and is utilized in both research and clinical areas since the early nineties. The most popular technique utilizes Blood Oxygenation Level Dependent (BOLD) contrast, which is based on the differing magnetic properties of oxygenated (diamagnetic) and deoxygenated (paramagnetic) blood. When brain neurons are activated, there is a

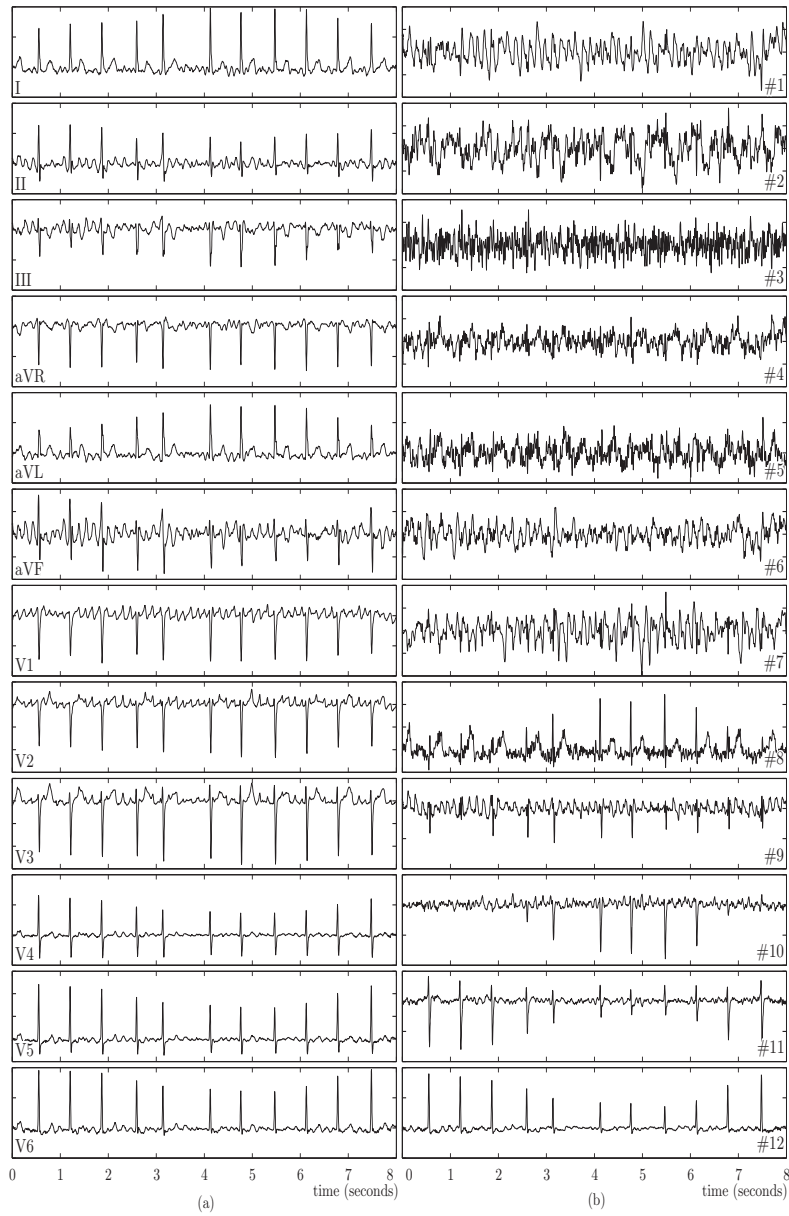


Figure 18.15: Inputs and results of the ICA separation process: (a) A 12-lead ECG from a patient in AF and (b) source estimates obtained by ICA and sorted from lower to higher kurtosis values. From [73] with permission.

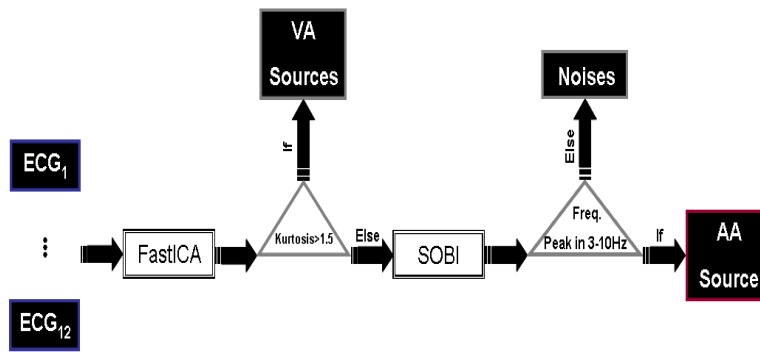


Figure 18.16: Block diagram of the spatio-temporal method proposed in [12].

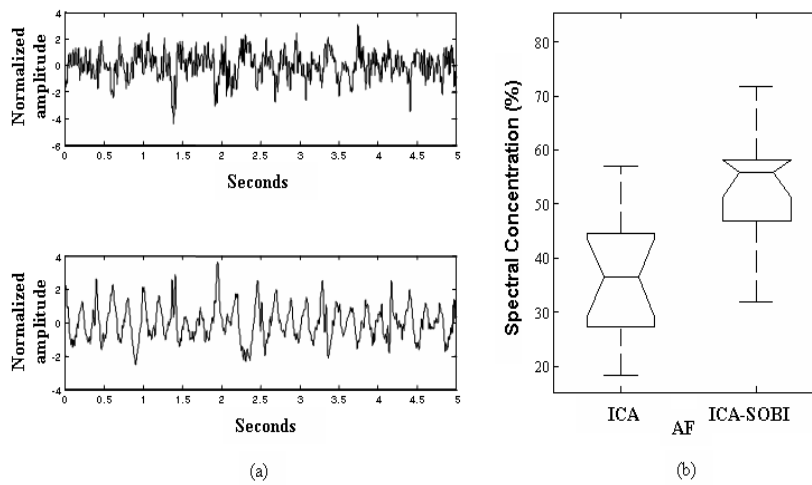


Figure 18.17: (a) An example where the spatio-temporal (ICA-SOBI) approach outperforms the spatial ICA and (b) spectral concentration of AA for AF. From [12] with permission.

resultant localized change in blood flow and oxygenation which causes a change in the MR decay parameter. These blood flow and oxygenation (vascular or hemodynamic) changes are temporally delayed relative to the neural firing, a confounding factor known as hemodynamic lag. Since the hemodynamic lag varies in a complex way from tissue to tissue, and because the exact transfer mechanism between the electrical and hemodynamic processes is not known, it is not possible to completely recover the electrical process from the vascular process. Nevertheless, the vascular process remains an informative surrogate for electrical activity. However, relatively low image contrast-to-noise ratio of the BOLD effect, head movement, and undesired physiological sources of variability (cardiac, pulmonary) make detection of the activation-related signal changes difficult. ICA has shown to be useful for fMRI analysis for several reasons. ICA finds systematically non-overlapping, temporally coherent brain regions without constraining the temporal domain. The temporal dynamics of many fMRI experiments are difficult to study with functional magnetic resonance imaging (fMRI) due to the lack of a well-understood brain-activation model. ICA can reveal inter-subject and inter-event differences in the temporal dynamics. A strength of ICA is its ability to reveal dynamics for which a temporal model is not available. ICA also works well for fMRI as it is often the case that one is interested in spatially distributed brain networks. A more exhaustive study of ICA for fMRI is proposed by Calhoun *et al.* [8].

Another, but not the last, application of ICA in biomedical engineering is its use in Magnetic Resonance Spectroscopy (MRS) contexts [70]. MRS is a recent diagnostic method that was adopted into clinical practice. As explained in [75], it consists in measuring different biochemical markers by tuning to particular nuclear resonance frequencies, thus providing precise characterization of tissue and/or a means for optimizing the SNR. It allows for the non-invasive characterization and quantification of molecular markers with clinical utility for improving detection, identification, and treatment for a variety of diseases, most notably brain cancers. The interpretation of MRS data is quite challenging: a typical dataset consists of hundreds of spectra, typically having low SNR with peaks that are numerous and overlapping. More particularly, the observed spectra are a combination of different constituent spectra. ICA can therefore be used to identify the shapes of the underlying constituent source spectra and their contribution to each voxel in the MRS data. Then its use aims at leading to a better quantification of each resonance peak.

Electromyographic (EMG) signal applications. These EMG signals acquired from skin electrodes may be generated by different muscles. It may overlap in the time and frequency domain, which make the classical filtering approaches less appropriate for EMG data separation. Farina *et al.* [28] show that, under certain assumptions, surface EMG may be considered as a linear instantaneous mixture. Experimental signals were collected by considering two muscles, the flexor carpi radialis and the pronator teres. The choice of these two muscles is motivated by the fact that, it is possible to produce contractions in which only one muscle is active at a time. The ICA method, proposed in [30], is then applied on three surface observations. The obtained results show that the source separation is not perfectly reached. The authors explain this limitation by the fact that the linear instantaneous mixture is just appropriate in the case of small muscles placed close to each other. Nevertheless, the reported results still very interesting show that ICA is a promising approach for surface EMG signals separation: the correlation coefficients between the separated sources and the reference sources (obtained by the arrays located directly over the muscles) is higher than 0.9.

18.3 Numerical complexity of ICA algorithms

Although the ultimate goal of a signal separation approach is the quality of such a separation, reflected on the estimated source signals, it is interesting to related the various ICA approaches from a numeral complexity viewpoint. Numerical complexity is defined here as the number of floating point operations required to execute an algorithm(flops). A flop corresponds to a multiplication followed by an addition. But, in practice, only the number of multiplications is considered since, most of the time, there are about as many (and slightly more) multiplications as additions. In order to simplify the expressions, the complexity is generally approximated by its asymptotic limit, as the size of the problem tends to infinity. We shall subsequently denote, with some small abuse of notation, the equivalence between two strictly positive functions f and g :

$$f(x) = \mathcal{O}[g(x)] \text{ or } g(x) = \mathcal{O}[f(x)] \quad (18.1)$$

if and only if the ratio $f(x)/g(x)$ tends to 1 as $x \rightarrow \infty$. In practice, knowing whether or not an algorithm is computationally costly becomes as important as knowing its performances in terms of SNR. Yet, despite its importance, the numerical complexity of the ICA algorithms is poorly addressed in the literature. This section first addresses the complexity of some elementary mathematical operations needed by ICA algorithms. Then, the numerical complexity of various ICA algorithms are reported and compared to each other as a function of the number of sources.

18.3.1 General tools

Many ICA algorithms use standard eigen-value decomposition (EVD) or singular value decomposition (SVD), for instance when a whitening step is required to reduce the dimensions of the space. Besides the latter decompositions, many operations can be considered as elementary such as solving a linear system, matrix multiplication, joint diagonalization of several matrices and computation of cumulants, when cumulant-based algorithms are considered.

- Let \mathbf{A} and \mathbf{B} be two matrices of size $(P \times N)$ and $(N \times P)$, respectively. Then the numerical complexity of their product $\mathbf{G} = \mathbf{AB}$ is equal to P^2N flops, since each element of \mathbf{G} requires N flops to be computed. The latter amount can be reduced to $(P^2 + P)N/2 = \mathcal{O}[P^2N/2]$ flops if \mathbf{G} is symmetric.
- The solution of a $P \times P$ linear system via the LU decomposition requires approximately $\mathcal{O}[4P^3/3]$ flops.
- The numerical complexity of the SVD of $\mathbf{A} = \mathbf{U}\mathbf{\Lambda}\mathbf{V}^T$ is given by $\mathcal{O}[2P^2N + 4PN^2 + 14N^3/3]$ flops when it is computed using the Golub-Reinsch algorithm [33]. This amount can be considerably reduced to $\mathcal{O}[2P^2N]$ when \mathbf{A} is tall (i.e. $P \gg N$) by resorting to Chan's algorithm [13], known to be suitable in such a case.
- The numerical complexity of the EVD $\mathbf{G} = \mathbf{L}\mathbf{\Sigma}\mathbf{L}^T$ is $\mathcal{O}[4P^3/3]$ flops.

Based on the previous expressions, the numerical SO whitening procedure is equal to $\mathcal{O}[TP^2/2 + 4P^3/3 + NPT]$ flops when it is achieved using the EVD while it is equal to $\mathcal{O}[2TP^2]$ flops when the SVD is considered.

Some ICA algorithms [7, 105, 10, 51, 30] are based on the joint approximate diagonalization of a set of M matrices \mathbf{G}_m ($1 \leq m \leq M$) of size $(P \times P)$. Recall that the joint diagonalization problem is defined as the search for a linear transformation that jointly diagonalizes the target matrices \mathbf{G}_m . Two main classes

of joint diagonalization techniques can be distinguished: the orthogonal and the non-orthogonal methods. The orthogonal joint diagonalization is defined when the diagonalizing matrix is unitary while the non-orthogonal one does not require such an assumption. A Jacobi-like algorithm such as the JADE algorithm [11] is commonly used for joint orthogonal diagonalization. Its numerical complexity is equal to $IP(P-1)(4PM+17M+4P+75)/2$ flops if the M matrices \mathbf{G}_m are symmetric where I stands for the number of executed sweeps. On the other hand, the ACDC algorithm [100] is a good choice when non-orthogonal joint diagonalization is concerned. The numerical complexity of the latter is given, for a full sweep AC phase with a single interlacing with the DC one, by $MNP^2+2P^3/3+(3P-1)/3+4N^3/3+(M+1)N^2P+(M+1)N^2+MNP^2$ flops per iteration.

Finally, regarding cumulants estimation, the computation of the $2q$ -th order cumulant of a P -dimensional random process requires $(2q-1)T$ flops where T stands for the data length. Consequently, the number of flops required to compute the $2q$ -th order cumulant array utilizing all its symmetries is then given by $(2q-1)Tf_{2q}(P)$ flops where $f_{2q}(P)$ denotes the number of its free entries and is given as a function of P , for $q=1,2,3$, by:

$$f_2(P) = \frac{P^2+P}{2} = \mathcal{O}\left[\frac{P^2}{2}\right] \quad (18.2)$$

$$f_4(P) = \frac{1}{8}P(P+1)(P^2+P+2) = \mathcal{O}\left[\frac{P^4}{8}\right] \quad (18.3)$$

$$f_6(N) = \frac{P^6}{72} + \frac{P^5}{12} + \frac{13P^4}{72} + \frac{P^3}{4} + \frac{22P^2}{72} + \frac{P}{6} = \mathcal{O}\left[\frac{P^6}{72}\right] \quad (18.4)$$

Table 18.1 summarizes the numerical complexities of the elementary operations considered in this chapter.

	Numerical complexity (flops)
$\mathbf{G} = \mathbf{AB}$	P^2N
Lin. system solving	$4P^3/3$
SVD of \mathbf{A}	$2P^2N+4PN^2+14N^3/3$
EVD of \mathbf{A}	$4P^3/3$
JAD [11] (Symmetric case)	$IP(P-1)(4PM+17M+4P+75)/2$
ACDC [100]	$(MNP^2+2P^3/3+(3P-1)/3+4N^3/3+(M+1)N^2P+(M+1)N^2+MNP^2)J_1$
Estimation of the $2q$ -th order cumulants array	$(2q-1)Tf_{2q}(P)$

Table 18.1: Numerical complexity of elementary operations generally used in the ICA methods. \mathbf{A} and \mathbf{B} are two matrices of size $(P \times N)$ and $(N \times P)$, respectively. I and M stand for the number of executed sweeps and the number of matrices to be jointly diagonalized, respectively. $f_{2q}(P)$ denotes the number of free entries in the $2q$ -th order cumulant array. J_1 is the number of iterations required for the convergence of the ACDC algorithm.

18.3.2 Complexity of several ICA algorithms

This section aims at giving insights into the numerical complexity of twelve ICA-based algorithms evaluated in this chapter, as a function of the number N of sources, the number P of sensors and the data length T . As mentioned in the introduction, these algorithms are JADE, COM2, SOBI, SOBI_{rob}, TFBSS, InfoMax, PICA, FastICA_{sym}, FastICA_{def}, FOBIUM_{ACDC}, SOBIUM and STOTD. Their numerical complexity are given in table 18.2.

Computational complexity	
	<p>P: number of sensors, N: number of sources, $J_i, i \in \{1, \dots, 6\}$ is the number of iterations in the iterative methods (PICA, InfoMax, FastICA_{sym}, FastICA_{def}, ALS-FIBI_{ACDC}). Q the complexity required to compute the roots of a real 4th degree polynomial by Ferrari's technique in the COM2 algorithm. L_w, N_t, N_f, M_1 and M_2 are respectively the smoothing window's length, the number of time bins, the number of frequency bins, the number of matrices referred to the time-frequency point wherein sources are of significant energy and the number of matrices among those M_1 ones with only one active source in the considered time-frequency point in the TFBSS algorithm. As far as the SOBIUM2 algorithm is concerned, m_1, n_1, m_2 and n_2 denote $\max(P^2, M)$, $\min(P^2, M)$, $\max(P^4, N(N+1)/2)$ and $\min(P^4, N(N+1)/2)$, respectively.</p>
SOBI _{rob}	$MT P^2/2 + 5M^2 P^3 - M^3 P^3/3 + 2MP^2 N + MN^2 P + MN^2 + (MN^2 + 4N^3/3)J_1 + MN + MP^2 + 2P^3/3 + PN + (3P - N)N^2/3 + IN(N-1)(17M + 75 + 4N + 4NM)/2$
SOBI	$MT P^2/2 + 4P^3/3 + (M-1)P^3/2 + IN(N-1)(17(M-1) + 75 + 4N + 4N(M-1))/2$
TFBSS	$\min(TP^2/2 + 4P^3/3 + NPT + N, 2TP^2) + 2N \log_2 N + N + (T + L_w + \log_2(L_w))N_t N_f N(N+1)/2 + 2M_1 N^3/3 + 3T_2 + IN(N-1)(4NM_2 + 17M_2 + 4N + 75)/2$
SOBIUM	$MT P^2/2 + \min(7m_1 n_1^2 + 11n_1^3/3, 3m_1 n_1^2) + 2P^2 N + P^2 N^2 + N(N-1)(4N^3/3 + N^4(N-1))/2 + 2N(N+1)P^4 + (2P^3/3 + (3P-1)/3)N + \min(7m_2 n_2^2 + 11n_2^3/3, 3m_2 n_2^2)$
COM2	$\min(TP^2/2 + 4P^3/3 + NPT, 2TP^2) + IN^2 Q/2 + \min(12If_4(N)N^2 + 2IN^3 + 3Tf_4(N) + TN^2, 13ITN^2/2)$
JADE	$\min(TP^2/2 + 4P^3/3 + NPT, 2TP^2) + 3Tf_4(N) + TN^2 + \min(4N^6/3, 8N^3(N^2 + 3)) + IN(N-1)(75 + 21N + 4N^2)/2$
STOTD	$\min(TP^2/2 + 4P^3/3 + NPT, 2TP^2) + 3TN^4/8 + 12IN^2(N^2 - 1)$
FOBIUM _{ACDC}	$3TMf_4(P) + (2P^6/3 + 2MNP^4 + (M+1)N^2P^2 + MN^2 + 4N^3/3 + N^2 + P^2)J_2 + NIP(P-1)(4P^2 + 21P + 75)/2$
PICA	$\min(TP^2/2 + 4P^3/3 + NPT, 2TP^2) + (N^3 + (T+1)N^2 + 3NT)J_3$
InfoMax	$\min(TP^2/2 + 4P^3/3 + NPT, 2TP^2) + (N^2 + N^3 + 4N + 5TN)J_4$
FastICA _{def}	$\min(TP^2/2 + 4P^3/3 + NPT, 2TP^2) + (2(N-1)(N+T) + 5TN(N+1)/2)J_5$
FastICA _{sym}	$\min(TP^2/2 + 4P^3/3 + NPT, 2TP^2) + 2P^3/2 + (16N^3/3 + N^2 + 3TN^2)J_6$

Table 18.2: Numerical complexity of some ICA-based algorithms

For a given number N of sources, the minimal numerical complexity of the previous methods is obtained by minimizing the values of I , P , M and T provided a good extraction of the sources is guaranteed. A good rule of thumb is to use at least $I_{\min} = 1 + \text{floor}(N^{1/2})$ sweeps as in [19]. The minimum value of P is equal to $P_{\min} = N$ for all the methods considered even if SOBIUM and FOBIUM_{ACDC} are able to identify underdetermined (i.e. $N > P$) mixtures of sources. We refer to chapter 9 for a treatment of under-determined mixtures. The minimum value of M is chosen equal to $M_{\min} = 6$ for SOBIUM, SOBI, SOBI_{rob} and FOBIUM_{ACDC}. The minimum value of T depends on several parameters such as N , P , the FO marginal cumulants and the SNR of sources. Therefore, it is chosen to be the same for all methods.

In summary, it is difficult to compare computational complexity across algorithms because the input parameters are different. But it is still possible if a common source extraction quality is imposed, which yields an estimation of the latter parameters. Another possibility would have been to impose a common overall numerical complexity for all methods as in [101, fig.1], and to look at performances.

In our experiment, these parameters are empirically estimated over 200 realizations in the context of the Mu-based BCI system described in section 18.4 when $P = 6$ sensors are used to recover $N = 2$ sources from $T = 10000$ data samples and for an SNR of 5 dB. Figure 18.18 shows the variations of the minimal numerical complexity of the twelve methods as a function of the number of sources N . In the sequel and for the sake of readability, all the methods considered are classified into three categories to be depicted in all figures: i) SO statistics methods (TFBSS, SOBIUM, SOBI and SOBI_{rob}), ii) HO cumulant-based methods (FOBIUM_{ACDC}, STOTD, COM2 and JADE) and iii) iterative MI-based methods (FastICA_{def}, FastICA_{sym}, PICA and InfoMax). The average number of iterations used in the iterative methods is equal to 6, 3, 17, 476 and 12 for FastICA_{def}, FastICA_{sym}, InfoMax, FOBIUM_{ACDC} and PICA, respectively. Regarding the TFBSS method, the number of used matrices M_1 and M_2 is equal to 8446 and 139 respectively while both the used number of time N_t and frequency N_f bins are set to $T/2$ with a smoothing window of size $N_f/10$. As depicted in figure 18.18, the TFBSS method requires generally the

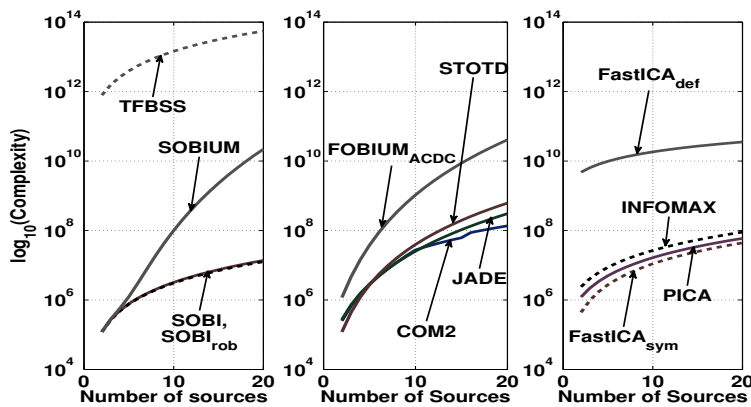


Figure 18.18: Minimal numerical complexity as a function of the number of sources for ten thousand data samples and SNR of 5 dB.

largest amount of calculations compared to the other methods followed by the FastICA_{def} one. Regarding the SOBIUM method, it shows an equivalent com-

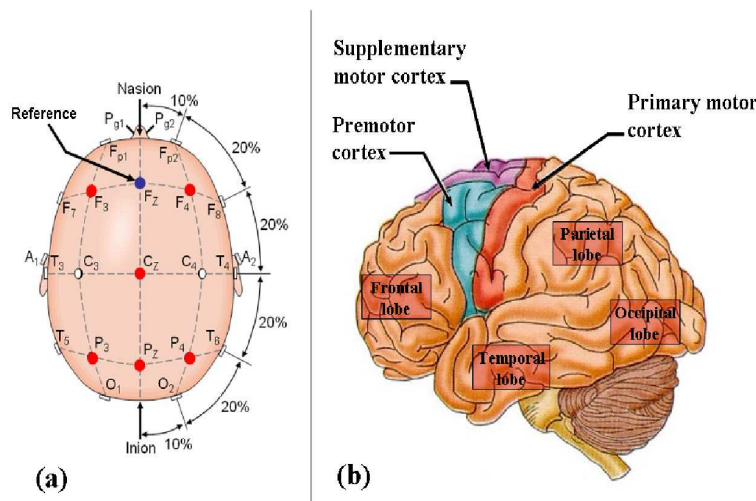


Figure 18.19: (a) The international 10-20 electrode placement system and (b) the surface of the left cerebral hemisphere, viewed from the side.

putational complexity compared to the ones of SOBI and SOBI_{rob} up to $N = 6$, while an important increase in its complexity can be noted beyond $N = 6$. FOBIUM_{ACDC} seems to be more costly than STOTD, COM2 and JADE where they show a comparable amount of calculations especially for $P < 10$. Finally, InfoMax, PICA and FastICA_{sym} show a comparable amount of calculations.

18.4 Performance analysis on biomedical signals

The goal of this section is to compare the performance of ICA methods on realistic biomedical signals. To do so, we will simulate EEG signals to be used for a brain-computer interface (BCI) system based on the Mu-rhythm with seven surface electrodes located around sensorimotor cortex (figure 18.19(a)). ICA-based BCI systems are now of great research interests thanks to potential of interpreting brain signals in real-time. So far only a limited set of ICA algorithms has been explored for this application [47], namely FastICA and InfoMax, whereas many other ICA-based algorithms could be used. This point is investigated by comparing the twelve aforementioned ICA algorithms, namely SOBI, SOBI_{rob}, COM2, JADE, TFBSS, FastICA_{def}, FastICA_{sym}, InfoMax, PICA, the STOTD and FOBIUM_{ACDC}.

In such a context the surface observations can be considered as a noisy mixture of one source of interest, namely the Mu-rhythm, and artifact sources such as the ocular activity. The intracerebral Mu wave located in the motor cortex (figure 18.19(b)) is simulated using the parametric model of Jansen [42] whose parameters are selected to derive a Mu-like activity. The ocular signal is obtained from our database. As far as the additive noise is considered, it is modeled as the sum of the instrumental noise and the background EEG activity. A Gaussian vector process is used to simulate the instrumental noise while a brain volume conduction of 800 independent EEG sources is generated using the Jansen model [42] in order to simulate a surface background EEG activity. Finally, the mixing matrix is defined as the concatenation of two columns modeling the head volume conduction [1] of the Mu and the ocular activities.

18.4.1 Comparative performance analysis on synthetic signals

Two studies are considered hereafter to evaluate the twelve ICA algorithms we have tested in the context of Mu-based BCI systems. In the first study, the quality of the source extraction is evaluated, as a function of the data samples for different SNR values. In the second study, the behavior of the ICA methods is examined in the case of an overestimation of the number of sources, for a fixed data length of $T = 10000$ and different SNR values. Moreover, the InfoMax algorithm is implemented with a prewhitening step. All reported results are obtained by averaging the performance criterion presented hereafter over 200 realizations. Note that a new trial of both sources and noise is generated at each realization.

18.4.1.1 Performance criterion

Two separators, $\mathbf{B}^{(1)}$ and $\mathbf{B}^{(2)}$ can be compared with the help of the criterion introduced by Chevalier [15]. The quality of the extracted component is directly related to its Signal to Interference-plus-Noise Ratio (SINR). More precisely, the SINR of the n -th source at the i -th output of the separator $\mathbf{B} = [\mathbf{b}_1, \dots, \mathbf{b}_N]$ is defined by:

$$\text{SINR}_n(\mathbf{b}_i) = \pi_n \frac{|\mathbf{b}_i^T \mathbf{A}_n|^2}{\mathbf{b}_i^T \mathbf{R}_\mathbf{x}^{(n)} \mathbf{b}_i} \quad (18.5)$$

where π_n represents the power of the n -th source, \mathbf{b}_i the i -th column of the separator \mathbf{B} and $\mathbf{R}_\mathbf{x}^{(n)}$ is the total noise covariance matrix for the n -th source, corresponding to the estimated data covariance matrix $\mathbf{R}_\mathbf{x}$ in the absence of the n -th source. On the basis of these definitions, the reconstruction quality of the n -th source at the output of the separator \mathbf{B} is evaluated by computing the maximum of $\text{SINR}_n(\mathbf{b}_i)$ with respect to i where $1 \leq i \leq N$. This quantity is denoted by $\text{SINRM}_n(\mathbf{B})$. The performance of a source separator \mathbf{B} is then defined by the following line vector $\text{SINRM}(\mathbf{B})$:

$$\text{SINRM}(\mathbf{B}) = (\text{SINRM}_1(\mathbf{B}), \dots, \text{SINRM}_N(\mathbf{B})) \quad (18.6)$$

In a given context, a separator $\mathbf{B}^{(1)}$ is better than another $\mathbf{B}^{(2)}$ for retrieving the source n , provided that $\text{SINRM}_n(\mathbf{B}^{(1)}) > \text{SINRM}_n(\mathbf{B}^{(2)})$. The criterion given by (18.6) allows for a quantitative performance evaluation and comparison of various ICA algorithms. However, the use of this criterion requires knowledge of its upper bound, which is achieved by the optimal source separator, in order to completely evaluate the performance of a given ICA method. It is shown in [15] that the optimal source separator corresponds to the separator $\mathbf{B}(\text{SMF})$ whose columns are the Spatial Matching Filters (SMF) associated with the different sources. It is defined to within a diagonal matrix and a permutation by $\mathbf{B}(\text{SMF}) = \mathbf{R}_\mathbf{x}^{-1} \mathbf{A}$ where \mathbf{A} is the true mixture.

18.4.1.2 Impact of both the SNR and the number of samples

Four experiments are realized in order to evaluate the behavior of the twelve ICA methods as a function of the data samples for different SNR values i.e. SNR = -5, 5, 15 and 25 dB. As depicted in figures 18.20, 18.21, 18.22 and 18.23, the SOBI_{rob} method exhibits, generally, quasi-optimal performance in extracting both sources (i.e. less than 1 dB from the optimal SINRM). Regarding the COM2, JADE, TFBSS, SOBI, $\text{FastICA}_{\text{def}}$, $\text{FastICA}_{\text{sym}}$, InfoMax, PICA and STOTD methods, their performance is comparable with a gap of 2 dB, approximately, from the optimal SINRM for SNR values less or equal to 15 dB. This gap is reduced for SNR of 25 dB and for sufficient data samples as shown in

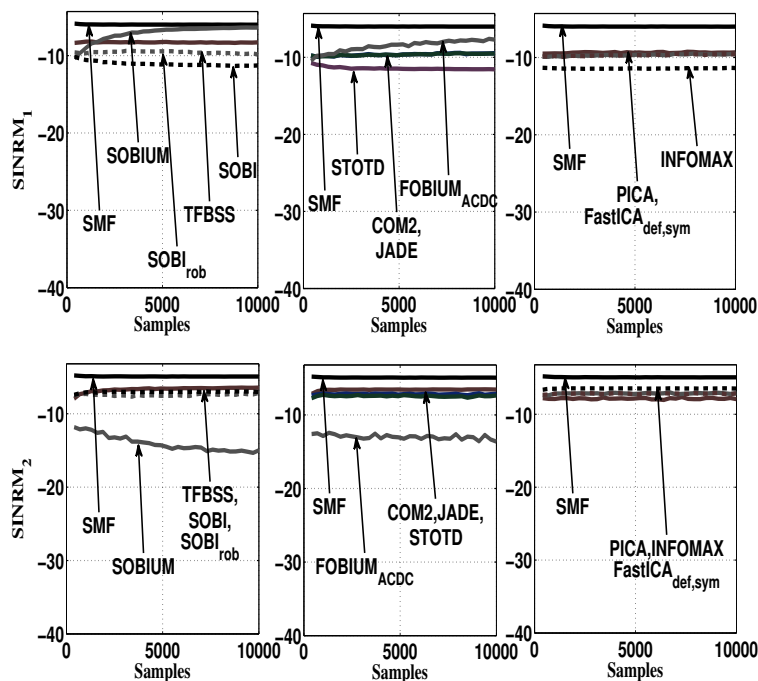


Figure 18.20: SINRM_n for $n \in \{1, 2\}$ as a function of the data samples with a SNR of -5 dB, at the output of twelve ICA methods in the context of Mu-based BCI systems. SINRM_1 and SINRM_2 express respectively the extraction quality measure of the ocular and the Mu activities compared to the optimal SMF filter. i) SO-cumulant based methods (left column), ii) HO cumulant-based methods (middle column) and iii) iterative MI-based methods (right column).

figure 18.23. Sometimes, the PICA algorithm suffers from convergence problems especially for a SNR of 5 dB as depicted in figure 18.21, which is probably due to the insufficiently small stop criterion, i.e. 10^{-4} . As far as the SOBIUM algorithm is concerned, its behavior seems to be comparable with the one of the SOBI_{rob} method for ocular activity extraction (i.e. SINRM_1). But, it shows a similar behavior as the ones of COM2, JADE, FastICA_{def} and FastICA_{sym} for the Mu wave extraction, except for a SNR of -5 dB which seems to strongly affect it. Finally the FOBIUM_{ACDC} algorithm shows a very good performance in extracting the ocular activity especially for low SNR values (figures 18.20 and 18.21) and small data samples where, in such a case, it outperforms the classical ICA methods such as COM2, JADE, FastICA_{sym} and FastICA_{def}. A comparable performance, but with a slower convergence speed, can be noted for the Mu wave extraction provided that the SNR is not too low because for a SNR of -5 dB, FOBIUM_{ACDC} shows a poor performance as compared to SOBIUM.

18.4.1.3 Impact of the overestimation of the number of sources

Since the estimation of the number of sources, when it is unknown, is essential in ICA methods, it should be interesting to examine the behavior of the latter when an overestimation of the number of sources occurs. Therefore, two experiments are realized showing the performance of the twelve methods as a function of the estimated number of sources, named N_{est} , for a true number of sources equal to 2 and for different SNR values, i.e. 5 dB and 25 dB.

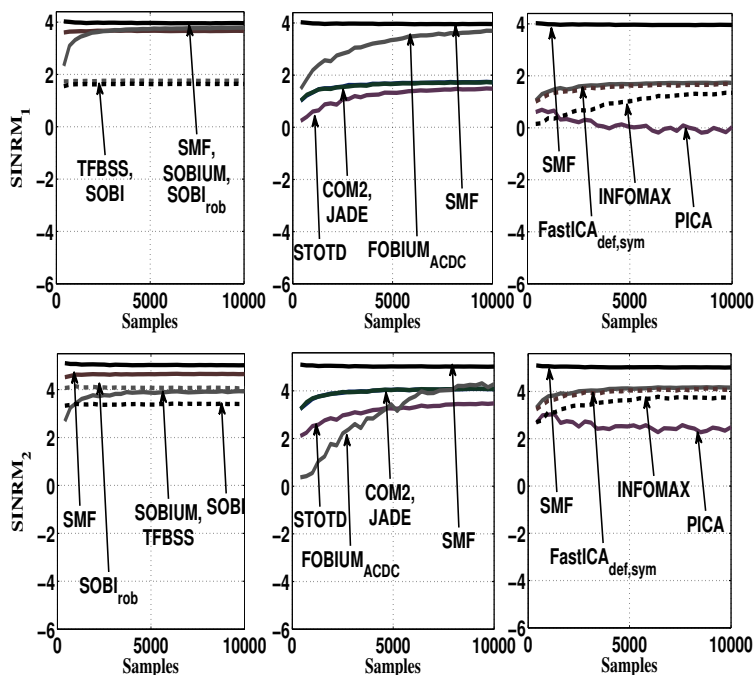


Figure 18.21: $SINRM_n$ for $n \in \{1, 2\}$ as a function of the data samples with a SNR of 5 dB, at the output of twelve ICA methods in the context of Mu-based BCI systems. $SINRM_1$ and $SINRM_2$ express respectively the extraction quality measure of the ocular and the Mu activities compared to the optimal SMF filter. i) SO-cumulant based methods (left column), ii) HO cumulant-based methods (middle column) and iii) iterative MI-based methods (right column).

For a SNR of 5 dB, figure 18.24 shows that the methods $SOBI_{rob}$, SOBI, COM2, JADE, TFBSS, $FastICA_{sym}$, $FastICA_{def}$ and STOTD, are insensitive to the overestimation of the number of sources. As far as the InfoMax and the $FOBIUM_{ACDC}$ algorithms are concerned, their behaviors are comparable, for ocular activity extraction, to those of the latter methods. In spite of this, they seem to be less effective when the Mu activity extraction (i.e. $SINRM_2$) is concerned, especially for the InfoMax method which shows a higher sensitivity. On the other hand, the performance of PICA can be considered as biased for an overestimation of the number of sources contrary to the latter methods, especially for the iterative ones such as $FastICA_{sym}$, $FastICA_{def}$, as shown in figure 18.24. Moreover, a comparable performance with the one of InfoMax can be noted for the PICA method, especially for Mu wave extraction. This behavior is probably due to the bias estimation of the moments required for the estimation of the Pearson model's parameters or to the high presence of noise which was probably extracted instead of the source of interest. Regarding the SOBIUM algorithm, it is the most affected by the overestimation of the number of sources as shown in Figure 18.24. Such a behavior may be explained by the miss-estimation of the subspace spanned by the matrices required for the joint diagonalization or, as for the PICA algorithm, by the high presence of noise that probably hides the source of interests. Thus, a good way to circumvent such a problem for both the SOBIUM and the PICA algorithms, is to extract as many sources as sensors. Such a solution guarantees the extraction of the sources of

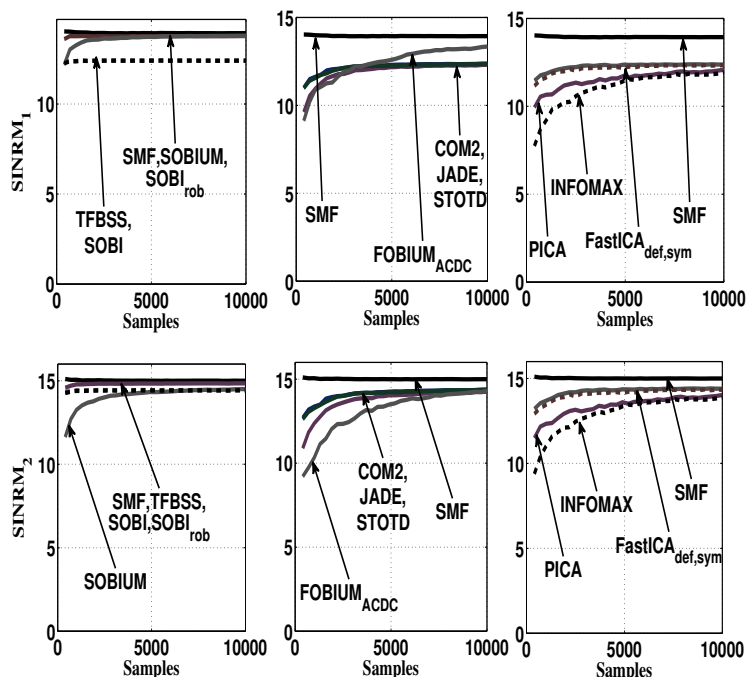


Figure 18.22: SINRM_n for $n \in \{1, 2\}$ as a function of the data samples with a SNR of 15 dB, at the output of twelve ICA methods in the context of Mu-based BCI systems. SINRM_1 and SINRM_2 express respectively the extraction quality measure of the ocular and the Mu activities compared to the optimal SMF filter. i) SO-cumulant based methods (left column), ii) HO cumulant-based methods (middle column) and iii) iterative MI-based methods (right column).

interest and enhance the source extraction quality as depicted in figures 18.24 and 18.25.

Finally, for a SNR of 25 dB, SOBI_{rob} , SOBI , PICA , SOBIUM , $\text{FOBIUM}_{\text{ACDC}}$, InfoMax show a quasi-similar behavior compared to the case of a SNR of 5 dB. But, contrary to the previous case, COM2 , STOTD , $\text{FastICA}_{\text{sym}}$, $\text{FastICA}_{\text{def}}$, JADE and TFBSS methods seem to be slightly sensitive to the overestimation of the number of sources, as depicted in figure 18.25 but with some superior performance of the COM2 and STOTD algorithms with respect to both JADE and TFBSS .

18.4.1.4 Summary of both studies

This section gives a summary of the computer results obtained from both previous studies. The main conclusions are as follows:

- SOBI_{rob} is the most powerful method compared to the other methods considered, especially those based on SO statistics. Its quasi-optimal performance (when its requested assumptions are satisfied) is not limited to source extraction with moderate numerical complexity, but also to its insensitivity to the overestimation of the number of sources.
- Regarding the HO cumulant-based methods, STOTD , COM2 and JADE show a good performance with moderate numerical complexity. One can

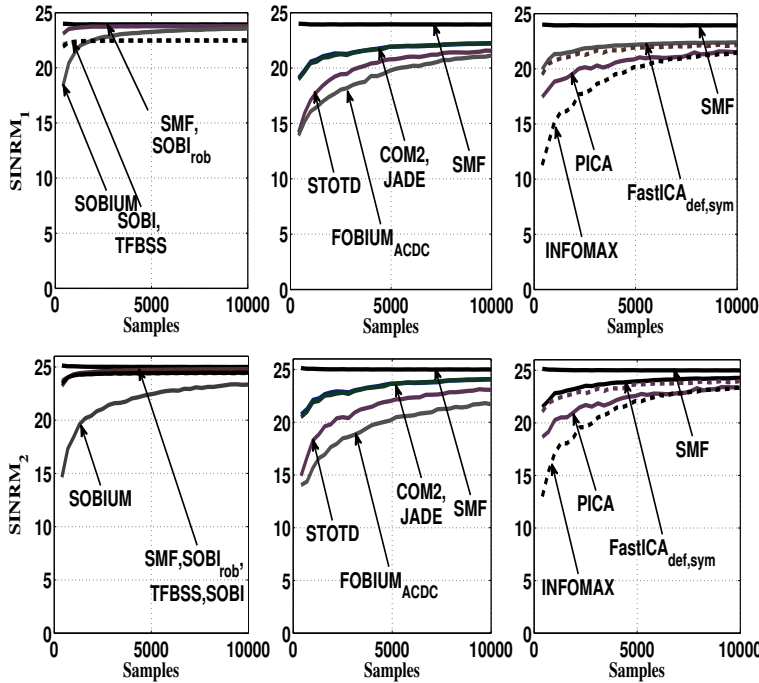


Figure 18.23: SINRM_n for $n \in \{1, 2\}$ as a function of the data samples with a SNR of 25 dB, at the output of twelve ICA methods in the context of Mu-based BCI systems. SINRM_1 and SINRM_2 express respectively the extraction quality measure of the ocular and the Mu activities compared to the optimal SMF filter. i) SO-based methods (left column), ii) HO cumulant-based methods (middle column) and iii) iterative MI-based methods (right column).

notice some weakness of the JADE algorithm with respect to an overestimation of the number of sources. On the other hand, one could resort to artifact removal as a preprocessing step (provided reasonable SNR) using the $\text{FOBIUM}_{\text{ACDC}}$ method, and then apply either COM2 or JADE or STOTD. It is worth noting that using reasonably small data samples for artifact removal would be a good trade-off between the performance and the computational complexity of the $\text{FOBIUM}_{\text{ACDC}}$ method.

- Both $\text{FastICA}_{\text{def}}$ and $\text{FastICA}_{\text{sym}}$ show generally a good performance for source extraction over the other iterative MI-based algorithm. But the $\text{FastICA}_{\text{sym}}$ algorithm should be preferred over the $\text{FastICA}_{\text{def}}$ when a constraint on the computational burden is imposed.

18.4.2 ICA of real data

In this section, we present an example of using ICA in the real data world. As we have already seen in our experiments, the SOBI_{rob} algorithm seems to be the most powerful method for simulated data. Therefore, it is applied to the observations depicted in figure 18.4. These observations present some surface electrical activities recorded by subset of 13 EEG electrodes, derived from the standardized 10-20 system during twenty second with a sampling rate of 256 Hz. Several artifact structures are evident, such as horizontal eye movements, eye blinks and muscle activity. In addition, other disturbances with

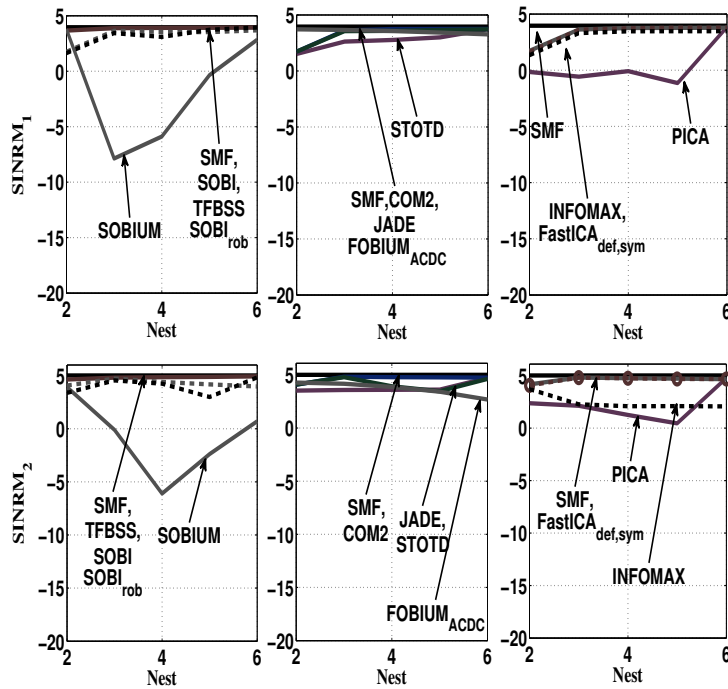


Figure 18.24: $SINRM_n$ for $n \in \{1, 2\}$ as a function of the estimated number of sources for a 10000 data samples and with a SNR of 5 dB at the output of twelve ICA methods in the context of Mu-based BCI systems. $SINRM_1$ and $SINRM_2$ express respectively the extraction quality measure of the ocular and the Mu activities compared to the optimal SMF filter. i) SO-cumulant based methods (left column), ii) HO-cumulant based methods (middle column) and iii) iterative methods (right column).

weaker power, such as electrode movements and baseline drift, contaminate the data. The obtained results, depicted in figure 18.26, show that components S3 and S5 represent clearly an activation of eye blinks and horizontal eye movements, respectively. Regarding the components S2 and S4, they represent the muscle activity and a slow movement which is probably related to the electrode movement. Besides, S1 displays the cerebral activity, which is considered in this experiment as the signal of interest. However, a slight alteration in S1, caused by eye blinks, still exists, which implies that the source extraction is not well-performed. This example shows that, even if the ICA can not perfectly separate the signal of interest from the artifacts, it guarantees the SNR enhancement.

18.5 Conclusion

The strength of ICA in the context of biomedical applications lies in its ability to extract signals despite the lack of reference signals or training labels. When this information is lacking, as is so often the case in biomedical signals, one can not use conventional regression methods to remove noise or extract signals of interest. ICA exploits the spatial diversity with which independent sources contribute additively to multiple simultaneous recordings. In all applications of ICA it is important to verify that the sources of interest do indeed satisfy these assumptions: diversity, independence, and linearity. For biomedical signals in

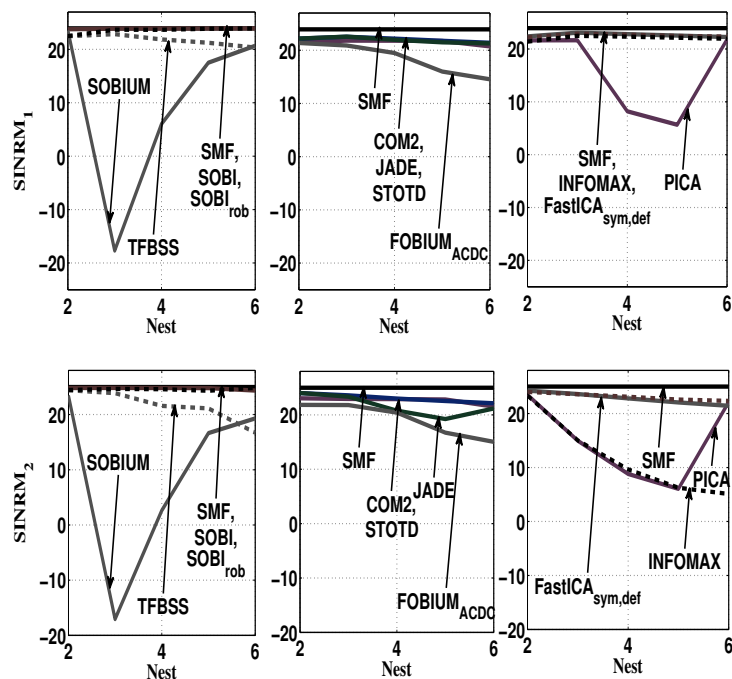


Figure 18.25: SINRM_n for $n \in \{1, 2\}$ as a function of the estimated number of sources for a 10000 data samples and with a SNR of 25 dB at the output of twelve ICA methods in the context of Mu-based BCI systems. SINRM_1 and SINRM_2 express respectively the extraction quality measure of the ocular and the Mu activities compared to the optimal SMF filter. i) SO-cumulant based methods (left column), ii) HO-cumulant based methods (middle column) and iii) iterative methods (right column).

particular, the use of ICA also imposes on the user the extra burden to demonstrate that the extracted components are physiologically meaningful. This is typically done by comparing the extracted sources to the known properties of the signals of interest such as their spatial distribution, spectral characteristics, or temporal regularities. This invariably requires the user to have a solid knowledge base in the specific biomedical domain. In summary, one could say that the power of ICA should be used responsibly.

Bibliography

- [1] L. ALBERA, A. FERREOL, D. COSANDIER-RIMELE, I. MERLET, AND F. WENDLING, *Brain source localization using a fourth-order deflation scheme*, IEEE Trans. Biomedical Eng., 55 (2008), pp. 490–501.
- [2] P. O. AMBLARD, M. GAETA, AND J. L. LACOUME, *Statistics for complex variables and signals – part II: signals*, Signal Processing, Elsevier, 53 (1996), pp. 15–25.
- [3] ———, *Statistics for complex variables and signals – parts I and II: Variables*, Signal Processing, Elsevier, 53 (1996), pp. 1–13.

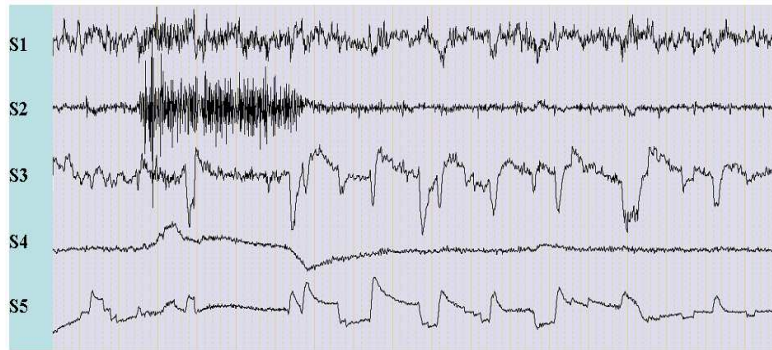


Figure 18.26: Result obtained by applying ICA to the signals depicted in figure 18.4.

- [4] S. BAILLET, J. C. MOSHER, AND R. M. LEAHY, *Electromagnetic brain mapping*, IEEE Signal Processing Magazine, 18 (2001), pp. 14–30.
- [5] A. K. BARROS, A. MANSOUR, AND N. OHNISHI, *Removing artefacts from electrocardiographic signals using independent component analysis*, Neurocomputing, 22 (1998), pp. 173–186.
- [6] M. BASSEVILLE, *Distance measures for signal processing and pattern recognition*, Signal Processing, 18 (1989), pp. 349–369.
- [7] A. BELOUHRANI, K. ABED-MERAIM, J. F. CARDOSO, AND E. MOULINES, *A blind source separation technique using second-order statistics*, IEEE Transactions On Signal Processing, 45 (1997), pp. 434–444.
- [8] V. D. CALHOUN, T. ADALI, L. K. HANSEN, J. LARSEN, AND J. J. PEKAR, *ICA of functional MRI data: An overview*, in ICA 03, Fourth International Symposium on Independent Component Analysis and Blind Signal Separation, Nara, Japan, April 1-4 2003, pp. 909–914.
- [9] J. F. CARDOSO, *Fetal electrocardiogram extraction by source subspace separation*, in IEEE International Conference on Acoustics Speech and Signal Processing, 1998, pp. 1941–1944.
- [10] J. F. CARDOSO AND A. SOULOUMIAC, *Blind beamforming for non-gaussian signals*, IEE Proceedings-F, 140, no. 6 (1993), pp. 362–370.
- [11] ———, *Jacobi angles for simultaneous diagonalization*, SIAM Journal Matrix Analysis and Applications, 17 (1996), pp. 161–164.
- [12] F. CASTELLS, J. J. RIETA, J. MILLET, AND V. ZARZOSO, *Spatiotemporal blind source separation approach to atrial activity estimation in atrial tachyarrhythmias*, IEEE Transactions on Biomedical Engineering, 52 (2005), pp. 258–267.
- [13] T. F. CHAN, *An improved algorithm for computing the singular value decomposition*, ACM Transaction on Mathematical Software, 8 (1982), pp. 72–83.
- [14] M. P. S. CHAWLA, H. K. VERMA, AND V. KUMAR, *Artifacts and noise removal in electrocardiograms using independent component analysis*, International Journal of Cardiology, 129 (2008), pp. 278–281.

- [15] P. CHEVALIER, *Optimal separation of independent narrow-band sources : Concept and Performances*, Signal Processing, Elsevier, 73 (1999), pp. 27–47.
- [16] M. K. CHUNG, *Current clinical issues in atrial fibrillation*, Cleveland Clinic Journal of Medicine, 70 (2003), pp. 6–11.
- [17] D. COHEN, *Magnetoencephalography: Evidence of magnetic fields produced by alpha rhythm currents*, Science, 161 (1972), pp. 664–666.
- [18] P. COMON, *Independent Component Analysis*, in Higher Order Statistics, J.-L. Lacoume, ed., Elsevier, Amsterdam, London, 1992, pp. 29–38.
- [19] ———, *Independent Component Analysis, a new concept ?*, Signal Processing, Elsevier, 36 (1994), pp. 287–314.
- [20] ———, *From source separation to blind equalization, contrast-based approaches*, in ICISP 01, International Conference on Image and Signal Processing, Agadir, Morocco, May 3-5 2001, pp. 20–32.
- [21] P. COMON AND E. MOREAU, *Improved contrast dedicated to blind separation in communications*, in ICASSP 97, 1997 IEEE International Conference on Acoustics Speech and Signal Processing, Munich, April 20-24 1997, pp. 3453–3456.
- [22] M. CONGEDO, C. GOUY-PAILLER, AND C. JUTTEN, *On the blind source separation of human electroencephalogram by approximate joint diagonalization of second order statistics*, Clinical Neurophysiology, 119 (2008), pp. 2677–2686.
- [23] L. DE LATHAUWER, D. CALLAERTS, B. DE MOOR, AND J. VANDEWALLE, *Fetal electrocardiogram extraction by source subspace separation*, in IEEE Workshop on Higher Order Statistics, Girona, Spain, June 12-14 1995, pp. 134–138.
- [24] L. DE LATHAUWER, B. DE MOOR, AND J. VANDEWALLE, *Fetal electrocardiogram extraction by blind source subspace separation*, IEEE Transactions on Biomedical Engineering, 47 (2000), pp. 567–572.
- [25] S. DEBENER, S. MAKEIG, A. DELORME, AND A. K. ENGEL, *What is novel in the novelty oddball paradigm? functional significance of the novelty P3 event-related potential as revealed by independent component analysis*, Cognitive Brain Research, 22 (2005), pp. 309–321.
- [26] K. L. DIAMANTARAS AND S. Y. KUNG, *Principal Component Neural Networks: Theory and Applications*, Adaptive and Learning Systems for Signal Processing, Communications and Control Series, John Wiley, New York, 1996.
- [27] L. FAES, G. NOLLO, E. O. M. KIRCHNER AND, F. GAITA, R. RICCARDI, AND R. ANTOLINI, *Principal component analysis and cluster analysis for measuring the local organization of human atrial fibrillation*, Medical and Biological Engineering and Computing, 39 (2001), pp. 656–663.
- [28] D. FARINA, C. FEVOTTE, C. DONCARLI, AND R. MERLETTI, *Blind separation of linear instantaneous mixtures of non-stationary surface myoelectric signals*, IEEE Transactions on Biomedical Engineering, 9 (2004), pp. 1555–1567.

- [29] A. FERREOL, L. ALBERA, AND P. CHEVALIER, *Fourth order blind identification of underdetermined mixtures of sources (FOBIUM)*, IEEE Transactions On Signal Processing, 53 (2005), pp. 1254–1271.
- [30] C. FEVOTTE AND C. DONCARLI, *Two contributions to blind sources separation using time-frequency distributions*, IEEE Signal processing Letters, 11 (2004), pp. 386–389.
- [31] A. FLEXER, H. BAUER, J. PRIPFL, AND G. DORFFNER, *Using ICA for removal of ocular artifacts in EEG recorded from blind subjects*, Neural Networks, 18 (2005), pp. 998–1005.
- [32] V. FUSTER, E. RYDEN, W. ASINGER, S. CANNOM, J. CRIJNS, R. L. FRYE, J. L. HALPERIN, G. N. KAY, W. W. KLEIN, S. LEVY, R. L. MCNAMARA, E. N. PRYSTOWSKY, L. S. WANN, AND D. G. WYSE, *Acc/aha/esc guidelines for the management of patients with atrial fibrillation*, Journal of the American College of Cardiology, 38 (2001), pp. 1266i–1266lxx.
- [33] G. H. GOLUB AND C. REINSCH, *Singular value decomposition and least squares solutions. In Handbook for Automatic computation II, Linear Algebra*, J. H. WILKINSON, Springer-Verlag, New York, 1970.
- [34] R. GUEVARA, J. L. VELAZQUEZ, V. NNADOVICE, R. WENNBERG, G. SENJANOVIC, AND L. G. DOMINGUEZ, *Phase synchronization measurements using electroencephalographic recordings: What can we really say about neuronal synchrony?*, Neuroinformatics, 3 (2005), pp. 301–314.
- [35] S. HAYKIN, ed., *Source separation: Models, concepts, algorithms and performance in Unsupervised Adaptive Filtering*, vol. I, Blind Source Separation of Series in Adaptive and Learning Systems for Communications, Signal Processing, and Control, Wiley, 2000.
- [36] A. HOLOBAR, C. FEVOTTE, C. DONCARLI, AND D. ZAZULA, *Single autotermes separation based on bilinear time-frequency representations*, in EUSIPCO, Toulouse, France, Septembre 2002, pp. 565–568.
- [37] S. HU, M. STEAD, AND G. A. WORRELL, *Automatic identification and removal of scalp reference signal for intracranial EEGs based on independent component analysis*, IEEE Transactions on Biomedical Engineering, 54 (2007), pp. 1560–1572.
- [38] A. HYVARINEN, *Fast and robust fixed-point algorithms for independent component analysis*, IEEE Transactions On Neural Networks, 10, no. 3 (1999), pp. 626–634.
- [39] A. HYVARINEN, J. KARHUNEN, AND P. OJA, *Independent component analysis*, Wiley interscience, Simon Haykin, 2001.
- [40] J. IRIARTE, E. URRESTARAZU, M. VALENCIA, M. ALEGRE, A. MALANDA, C. VITERI, AND J. ARTIEDA, *Independent component analysis as a tool to eliminate artifacts in EEG: A quantitative study*, Journal of Clinical Neurophysiology, 20 (2003), pp. 249–257.
- [41] C. J. JAMES AND O. J. GIBSON, *Temporally constrained ICA: An application to artifact rejection in electromagnetic brain signal analysis*, IEEE Transaction on Biomedical Engineering, 50 (2003), pp. 1108–1116.
- [42] B. H. JANSEN AND V. G. RIT, *Electroencephalogram and visual evoked potential generation in a mathematical model of coupled cortical columns?*, Biological Cybernetics, 73 (1995), pp. 357–366.

- [43] C. A. JOYCE, I. F. GORODNITSKY, AND M. KUTAS, *Automatic removal of eye movement and blink artifacts from EEG data using blind component separation*, *Psychophysiology*, 41 (2004), pp. 313–325.
- [44] T.-P. JUNG, S. MAKEIG, M. WESTERFIELD, J. TOWNSEND, E. COURCHESNE, AND T. J. SEJNOWSKI, *Removal of eye activity artifacts from visual event-related potentials in normal and clinical subjects*, *Clinical Neurophysiology*, 11 (2000), pp. 1754–1758.
- [45] ———, *Analysis and visualization of single-trial event-related potentials*, *Human Brain Mapping*, 14 (2001), pp. 166–185.
- [46] M. JUNGHOFER, T. ELBERT, D. M. TUCKER, AND C. BRAUN, *The polar average reference effect: A bias in estimating the head surface integral in EEG recording*, *Clinical Neurophysiology*, 110 (1999), pp. 1149–1155.
- [47] A. KACHENOURA, L. ALBERA, L. SENHADJI, AND P. COMON, *ICA: a potential tool for BCI systems*, *IEEE Signal Processing Magazine*, special issue on Brain-Computer Interfaces, 25 (2008), pp. 57–68.
- [48] J. KARVANEN AND V. KOIVUNEN, *Blind separation methods based on pearson system and its extensions*, *Signal Processing*, Elsevier, 82 (2002), pp. 663–673.
- [49] J. L. LACOUME, P. O. AMBLARD, AND P. COMON, *Statistiques d'ordre supérieur pour le traitement du signal*, Collection Sciences de l'Ingénieur, Masson, 1997.
- [50] P. LANGLEY, J. P. BOURKE, AND A. MURRAY, *Frequency analysis of atrial fibrillation*, in *IEEE Computers in Cardiology*, 2000, pp. 65–68.
- [51] L. D. LATHAUWER AND J. CASTAING, *Blind identification of underdetermined mixtures by simultaneous matrix diagonalization*, *IEEE Transactions on Signal Processing*, 56 (2008).
- [52] L. D. LATHAUWER, B. D. MOOR, AND J. VANDEWALLE, *Independent component analysis and (simultaneous) third-order tensor diagonalisation*, *IEEE Transactions on Signal Processing*, 49 (2001), pp. 2262–2271.
- [53] T. W. LEE, M. GIROLAMI, AND T. J. SEJNOWSKI, *Independent component analysis using an extended infomax algorithm for mixed sub-gaussian and super-gaussian sources*, *Neural Computation*, 11 (1999), pp. 417–441.
- [54] R. LEGARRETA, *Component selection for pca-based extraction of atrial fibrillation*, in *IEEE Computers in Cardiology*, 2006, pp. 137–140.
- [55] S. LEVY, G. BREITHARDT, R. W. F. CAMPBELL, A. J. CAMM, J. C. DAUBERT, M. ALLESSIE, E. ALIOT, A. CAPUCCI, F. COSIO, H. CRIJNS, L. JORDAENS, R. N. W. HAUER, F. LOMBARDI, AND B. LDERITZ, *Atrial fibrillation : Current knowledge and recommendations for management*, *European Heart Journal*, 419 (1998), pp. 91294–1320.
- [56] S. MAKEIG, A. J. BELL, T.-P. JUNG, AND T. J. SEJNOWSKI, *Independent component analysis of electroencephalographic data*, *Advances in Neural Information Processing Systems*, 8 (1996), pp. 145–151.
- [57] S. MAKEIG, T.-P. JUNG, A. J. BELL, D. GHADERMANI, AND T. J. SEJNOWSKI, *Blind separation of auditory event-related brain responses into independent components*, *Proceedings of National Academy of Science of the United States of America*, 94 (1997), pp. 10979–10984.

- [58] J. MALMIVIO AND R. PLONSEY, *Bioelectromagnetism*, Principles and Applications of Bioelectric and Biomagnetic Fields, Oxford University Press, New York, 1995.
- [59] P. MCCULLAGH, *Tensor Methods in Statistics*, Chapman and Hall, Monographs on Statistics and Applied Probability, 1987.
- [60] M. J. MCKEOWN, S. MAKEIG, G. B. BROWN, T. B. JUNG, S. S. KINDERMANN, A. J. BELL, AND T. J. SEJNOWSKI, *Analysis of fMRI data by blind separation into independent spatial components*, Human Brain Mapping, 6 (1998), pp. 160–188.
- [61] M. J. MCKEOWN AND T. J. SEJNOWSKI, *Independent component analysis of fMRI data: Examining the assumptions*, Human Brain Mapping, 6 (1998), pp. 368–372.
- [62] J. C. MOSHER AND R. M. LEAHY, *Source localization using Recursively Applied and Projected (RAP) music*, IEEE Transactions On Signal Processing, 47 (1999), pp. 332–340.
- [63] J. L. ONTON, A. DELORME, AND S. MAKEIG, *Frontal midline EEG dynamics during working memory*, Neuroimage, 27 (2005), pp. 341–356.
- [64] T. OOSTENDORP, *Modeling the Fetal ECG*, PhD thesis, K. U. Nijmegen, 1989.
- [65] A. OSSADTCHI, S. BAILLET, J. C. MOSHER, D. THYERLEID, W. SUTHERLINGD, AND R. M. LEAHY, *Automated interictal spike detection and source localization in magnetoencephalography using independent components analysis and spatio-temporal clustering*, Clinical Neurophysiology, Elsevier, 115 (2004), pp. 508–522.
- [66] M. I. OWIS, A. B. M. YOUSSEF, AND Y. M. KADAH, *Characterization of ecg signals based on blind source separation*, Medical and Biological Engineering and Computing, 40 (2002), pp. 557–564.
- [67] ———, *A successive cancellation algorithm for fetal heartrate estimation using an intrauterine ecg signal*, IEEE Transactions on Biomedical Engineering, 49 (2002), pp. 943–954.
- [68] R. PLONSEY, *Bioelectric phenomena*, McGraw-Hill, New York, 1969.
- [69] F. POREE, A. KACHENOURA, H. GAUVRIT, C. MORVAN, G. CARRAULT, AND L. SENHADJI, *Blind source separation for ambulatory sleep recording*, Transactions on Information Technology in Biomedicine, 10 (2006), pp. 293–301.
- [70] J. PULKKINEN, A. M. HKKINEN, N. LUNDBOM, A. PAETAU, R. A. KAUPPINEN, AND Y. HILTUNEN, *Independent component analysis to proton spectroscopic imaging data to human brain tumours*, European Journal of Radiology, 56 (2005), pp. 160–164.
- [71] R. M. RANGAYYAN, *Biomedical signal analysis: A case study approach*, IEEE Press Series on Biomedical Engineering, John Wiley, New York, 2002.
- [72] J. J. RIETA, F. CASTELLS, C. SANCHEZ, AND J. IGUAL, *Ica applied to atrial fibrillation analysis*, in International Conference of Independent Component Analysis and Blind Signal Separation, 2003, pp. 59–64.

- [73] J. J. RIETA, F. CASTELLS, C. SANCHEZ, V. ZARZOZO, AND J. MILLET, *Atrial activity extraction for atrial fibrillation analysis using blind source separation*, IEEE Transactions on Biomedical Engineering, 51 (2004), pp. 1176–1186.
- [74] J. J. RIETA, V. ZARZOSO, J. MILLET, R. GARCIS, AND R. RUIZ, *Atrial activity extraction based on blind source separation as an alternative to qrst cancellation for atrial fibrillation analysis*, in IEEE Computers in Cardiology, 2000, pp. 69–72.
- [75] P. SAJDA, S. DU, T. BROWN, R. STOYANOVA, D. SHUNGU, X. MAO, AND L. PARRA, *Nonnegative matrix factorization for rapid recovery of constituent spectra in magnetic resonance chemical shift imaging of the brain*, IEEE Transactions on Medical Imaging, 23 (2004), pp. 1453–1465.
- [76] R. SAMENI, *Extraction of fetal cardiac signals from an array of maternal abdominal recordings*, PhD thesis, Institut Polytechnique de Grenoble, July 2008.
- [77] C. SANCHEZ, J. MILLET, J. J. RIETA, F. CASTELLS, J. RODENAS, R. RUIZ, AND V. RUIZ, *Packet wavelet decomposition: An approach for atrial activity extraction*, in IEEE Computers in Cardiology, 2002, pp. 33–36.
- [78] S. J. SCHIFF, *Dangerous phase*, Neuroinformatics, 3 (2006), pp. 315–318.
- [79] L. SORNMO AND P. LAGUNA, *Bioelectrical signal processing in cardiac and neurological applications*, Biomedical Engineering, Elsevier, Academic Press, USA, 2005.
- [80] M. STRIDH AND L. SRNMO, *Spatiotemporal qrst cancellation techniques for analysis of atrial fibrillation*, IEEE Transactions on Biomedical Engineering, 48 (2001), pp. 105–111.
- [81] E. M. SYMONDS, D. SAHOTA, AND A. CHANG, *Fetal electrocardiography*, Cardiopulmonary medicine, Imperial College Press, London, 2001.
- [82] H. TAIGANG, G. CLIFFORD, AND L. TARASSENKO, *Application of independent component analysis in removing artefacts from the electrocardiogram*, Neural Computing and Applications, 15 (2006), pp. 105–116.
- [83] T. TALMON, J. KORS, AND J. VON, *Adaptive gaussian filtering in routine ecg/vcg analysis*, IEEE Transactions On Acoustics, Speech and Signal Processing, 34 (1986), pp. 527–534.
- [84] A. C. TANG, B. A. PEARLMUTTER, N. A. MALASZENKO, AND D. B. PHUNG, *Independent components of magnetoencephalography: Single-trial response onset times*, NeuroImage, 17 (2002), pp. 1773–1789.
- [85] A. C. TANG, B. A. PEARLMUTTER, N. A. MALASZENKO, D. B. PHUNG, AND B. C. REEB, *Independent components of magnetoencephalography: Localization*, Neural Computation, 14 (2002), pp. 1827–1858.
- [86] N. THAKOR AND Z. YI-SHENG, *Applications of adaptive filtering to ecg analysis : noise cancellation and arrhythmia detection*, IEEE transactions on biomedical engineering, 38 (1991), pp. 785–794.
- [87] C. VASQUEZ, A. I. HERNANDEZ, F. MORA, G. CARRAULT, AND G. PAS-SARIELLO, *Atrial activity enhancement by wiener filtering using an artificial neural network*, IEEE Transactions On Biomedical Engineering, 48 (2001), pp. 940–944.

- [88] R. VETTER, N. VIRAG, J. M. VESIN, P. CELKA, AND U. SCHERRER, *Observer of autonomic cardiac outflow based on blind source separation of ECG parameters*, IEEE Transactions On Biomedical Engineering, 47 (2000), pp. 578–582.
- [89] R. VIGARIO, *Extraction of ocular artefacts from EEG using independent component analysis*, Electroencephalography Clinical Neurophysiology, 103 (1997), pp. 395–404.
- [90] R. VIGARIO, V. JOUSMAKI, M. HAMALAINEN, R. HARI, AND E. OJA, *Independent component analysis for identification of artifacts in magnetoencephalographic recordings*, in Proceedings of the 1997 conference on Advances in Neural Information Processing System 10, MIT Press Cambridge, MA, USA, Denver, USA, 1998, pp. 229–235.
- [91] R. VIGARIO AND E. OJA, *Bss and ica in neuroinformatics: From current practices to open challenges*, IEEE Reviews in Biomedical Engineering, 1 (2008), pp. 50–61.
- [92] R. VIGARIO, J. SARELA, V. JOUSMAKI, M. HAMALAINEN, AND E. OJA, *Independent component approach to the analysis of EEG and MEG*, IEEE Transactions On Biomedical Engineering, 47 (2000), pp. 589–593.
- [93] R. VIGARIO, J. SREL, V. JOUSMKI, AND E. OJA, *Independent component analysis in decomposition of auditory and somatosensory evoked fields*, in ICA'99, Second International Symposium on Independent Component Analysis and Blind Signal Separation, Aussois, France, Jan. 1999, pp. 167–172.
- [94] R. VIGARIO, A. ZIEHE, K.-. MULLER, G. WUBBELER, L. TRAHMS, B. M. MACKERT, G. CURIO, V. JOUSMAKI, J. SARELA, AND E. OJA, *Blind decomposition of multimodal evoked responses and DC fields*, MIT Press, Cambridge, MA, USA, 2003.
- [95] J. A. WESTGATE, A. J. GUNN, L. BENNET, M. I. GUNNING, H. H. D. HAAN, AND P. D. GLUCKMAN, *Do fetal electrocardiogram pr-rr changes reflect progressive asphyxia after repeated umbilical cord occlusion in fetal sheep?*, Pediatric Research, 44 (1998), pp. 419–461.
- [96] B. WIDROW, J. GLOVER, J. MCCOOL, J. KAUNITZ, C. WILLIAMS, H. HEARN, J-ZEIDLER, E. DONG, AND R. GOOGLIN, *Adaptive noise cancelling: principles and applications*, Proc. IEEE, 63 (1975), pp. 1692–1716.
- [97] T. WINSOR, *Primer of vectorcardiography*, Lea and Febiger, Philadelphia, 1972.
- [98] J. O. WISBECK, A. K. BARROS, AND R. OJEDA, *Application of ica in the separation of breathing artefacts in ECG signals*, in International Conference on Neural Information Processing, (ICONIP'98), 1998, pp. 211–214.
- [99] J. O. WISBECK AND R. G. OJEDA, *Application of neural networks to separate interferences and ecg signals*, in Proceedings of the 1998 Second IEEE International Caracas Conference, 1998, pp. 291–294.
- [100] A. YEREDOR, *Non-orthogonal joint diagonalization in the least-squares sense with application in blind source separation*, IEEE Transactions On Signal Processing, 50 (2002), pp. 1545–1553.

- [101] V. ZARZOSO AND P. COMON, *Comparative speed analysis of FastICA*, in ICA'07, M. E. Davies, C. J. James, S. A. Abdallah, and M. D. Plumbley, eds., vol. 4666 of Lecture notes in Computer Sciences, London, UK, Sept. 9-12 2007, Springer, pp. 293–300.
- [102] ———, *Robust independent component analysis for blind source separation and extraction*, in International IEEE Engineering in Medicine and Biology Conference, 2008, pp. 3344–3347.
- [103] V. ZARZOSO AND A. K. NANDI, *Blind separation of independent sources for virtually any source probability density function*, IEEE Transactions on Signal Processing, 47 (1999), pp. 2419–2432.
- [104] V. ZARZOSO, A. K. NANDI, AND E. BACHARAKIS, *Noninvasive fetal electrocardiogram extraction: blind separation versus adaptative noise cancellation*, IEEE Transactions on Biomedical Engineering, 48 (2001), pp. 12–18.
- [105] A. ZIEHE AND K. R. MULLER, *TDSEP - an efficient algorithm for blind separation using time structure*, in ICANN'98, Proceedings of the 8th International Conference on Artificial Neural Networks, 1998, pp. 675–680.